Doctoral Thesis

Analysis of Solar Irradiance Fluctuations for Photovoltaic Module Outdoor Performance Testing

太陽光発電モジュール屋外性能評価に係る日射変動解析

2018

Environmental and Renewable Energy Systems Division

Graduate School of Engineering

Gifu University

Junfang Zhang

Contents

Chapter 1 Introduction

1.1 Background

In 2015, The United Nations General Assembly adopted a dedicated Sustainable Development Goal on Sustainable Energy in order to o keep global temperature rise well below 2 degrees Celsius. Therefore, clear renewable energy and high-efficient energy took more and more attentions around the world, and the global energy mix is shifting towards cleaner, lower carbon fuels in recently years. According to the Renewables 2017 Global Status Report, the total capacity of renewable energy in 2015 was 1856 gigawatts (GW), and a greatest increase in renewable energy capacity in 2016, 9% compared to 2015, about 161 GW of capacity, by 2017 GW . Particular, the growth of solar photovoltaic is remarkable, accounted for 47% of newly installed renewable power capacity in 2016. At least 75 GW of solar PV system have been installed and connected to the gird of the world in 2016, and the total cumulative installed capacity of solar PV power reach 303 GW. Asia ranks in first place for the fourth year in a row with around 67% of the global PV market, up from 60% last year. A significantly growing occurred in China, reached 34.54 GW in 2016, is the leader in terms of total capacity with 78 GW as shown in Fig. 1.2. On the other hand, in Japan, the renewable energy market has greatly grown, and introduction of renewable energy mainly in solar PV has started in each area since March, 11, 2011. The growth of solar PV in Japan has a declining tendency compared with previous with around 8,6 GW installed and connected to the grid in 2016. Nevertheless, the cumulative installed capacity in Japan reached 42.8 GW, becoming the second largest country in the world at the end of 2016.

With the great growth and expansion of the global solar market, it is essential to develop a common technic such as the reliability and safety in long-term and the technology of PV

module performance testing for new type PV module is also necessary.

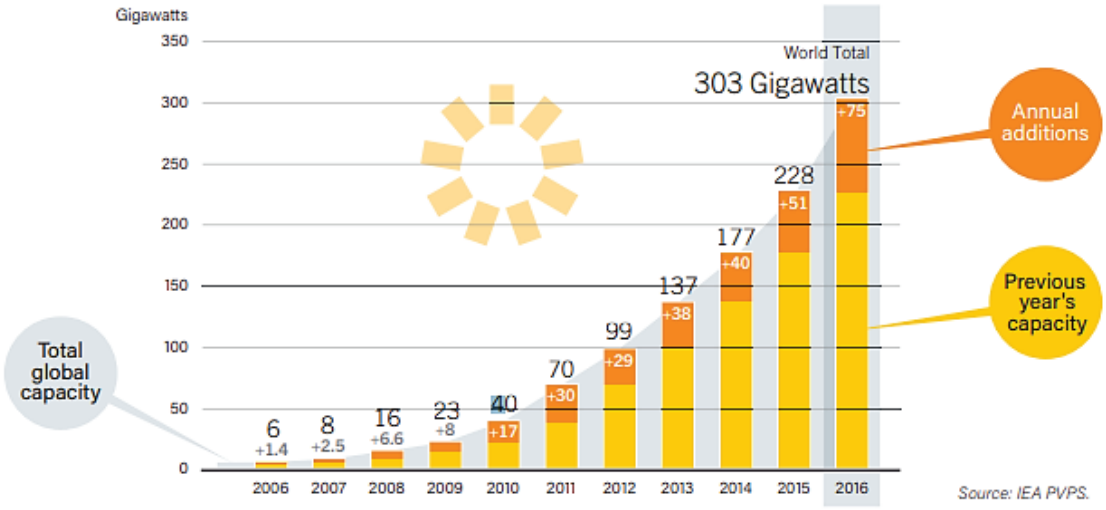

Fig. 1.1 Solar PV Global Capacity and Annual Additions, 2006-2016

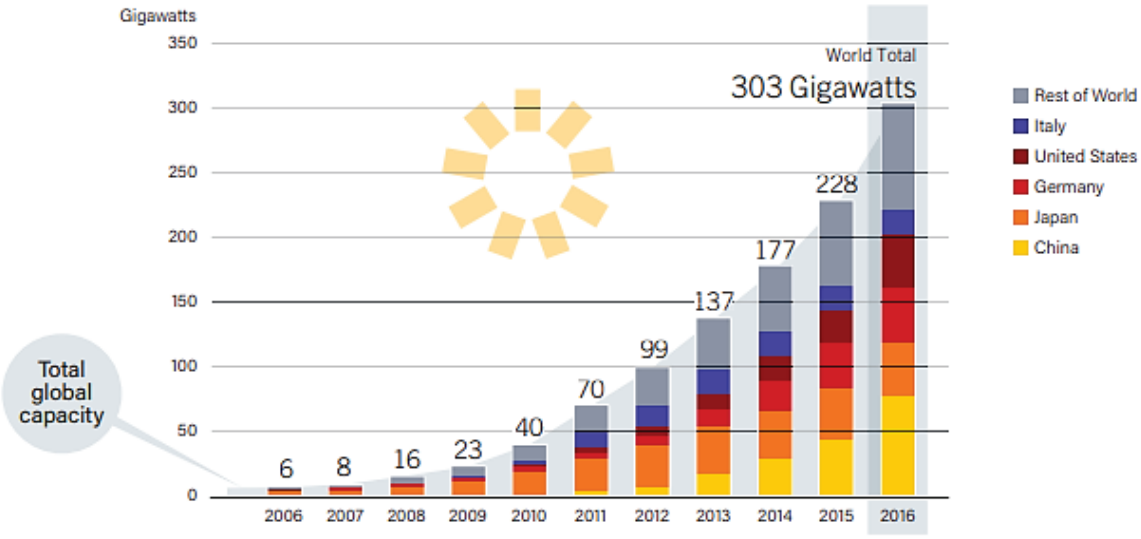

Fig. 1.2 Solar PV Global Capacity, by Country and Region, 2006-2016

1.2 Objective and outline of this thesis

The objective of this study is to analyze the characterization of solar irradiance fluctuations in a short period which corresponding to the period of a high-speed I-V testing that a way is used to evaluated the performance of PV modules. The characterizations of solar irradiance fluctuation under different clouds conditions are analyzed in temporal instability and nonuniformity, respectively in this research. Moreover, a filter method is proposed in here which can select the suitable events that satisfied the conditions with stable solar irradiance in time and space for high-accuracy outdoor PV module performance only with a single PV module performance. This paper consists of 7 charters and a brief introduction as follows.

Chapter 1 introduces the background and status of PV system, and the objective of this study. Chapter 2 introduces the method for PV module performance testing and states the observation system employed in this study. Chapter 3 analyzed fluctuations of solar irradiance in a short-period 1 s, the frequency distribution of rate change for solar irradiance in 1 s is described in here and the seasonal differences of solar fluctuation are also discussed. The event of extreme fluctuation of irradiance due to cloud movement also has been enumerated. Chapter 4 analyzes the temporal instability and nonuniformity of solar irradiance under clouds. Travelling speed and direction of cloud shadows on PVMSs are evaluated from the fluctuations of irradiance observed by several PVMSs. Cloud distributions are classified into four cloud types, and the characteristics of the solar irradiance fluctuations are discussed for each type. Chapter 5 presents the enhancement of solar irradiance caused by the edges effect of clouds. The mechanism of cloud edge effect and the corresponding weather conditions also were indicated in this chapter. Meanwhile, events with enhanced solar irradiances were

detected for three months and were analyzed statistically. Chapter 6 proposed a filter method to detect the events in which irradiance is stable and uniform for PV module outdoor performance characterization with a single meter. Relationships of instability and nonuniformity of irradiance to measurement conditions are discussed, e.g. longer measurement time makes instability worse. Furthermore, the filter method under various weather conditions also has been discussed in this chapter. Finally, the conclusions of the whole study are given in Chapter 7.

Reference

1. Renewables 2017 Global Status Report - REN21
2. IEA-PVPS Annual Report 2017
3. http://solar-support.co.jp/i-v.html

Chapter 2 Experimental method and observation system

2.1 PV module performance testing

PV module performance testing is essential to evaluate the characterizations and situations of PV module new produced or installed already for its reliability and safety in long-term. In general, there are two common indexes to describe the PV module performance, equipment capacity and conversion efficiency. Equipment capacity is the total value of the nominal maximum output of modules. The nominal maximum output of modules is determined according to the maximum output under the common measurement condition. The conversion efficiency of a solar cell is a parameter which is defined by the faction of incident power converted into electricity. In general, the PV module performance testing procedure indicates the current-voltage (I-V) measurement when sunlight illuminates a solar cell and the change the variable resistance in the range from 0 Ω to unlimited. The measurement principle and circuit diagram is shown in Fig. 2.1.

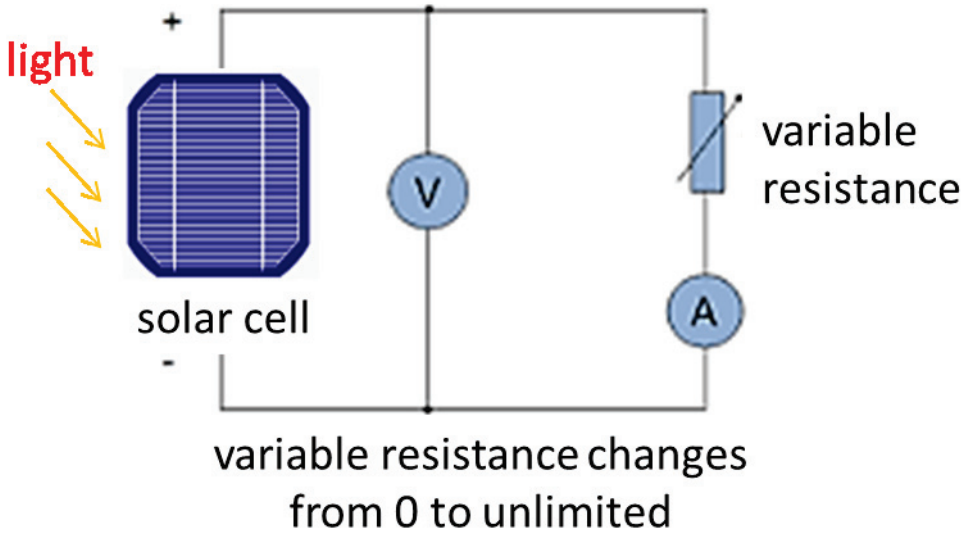

Fig. 2.1 The measurement principle and circuit diagram of I-V curve measurement

An example image of current-voltage curve is shown in Fig. 2.2. The parameters of short-circuit current I_{sc}, open-circuit V_{oc}, and maximum power point P_m are measured in this figure. The current is proportional to light intensity, and the voltage relates to the operation cell temperatures. In this figure, two I-V curve lines were descripted, and the red line shows a normal I-V curve measurement. But an abnormal I-V curve also be measured as the green line shown, due to a significant part of loss in performance is caused by a variation in sunlight, and operating cell temperatures.

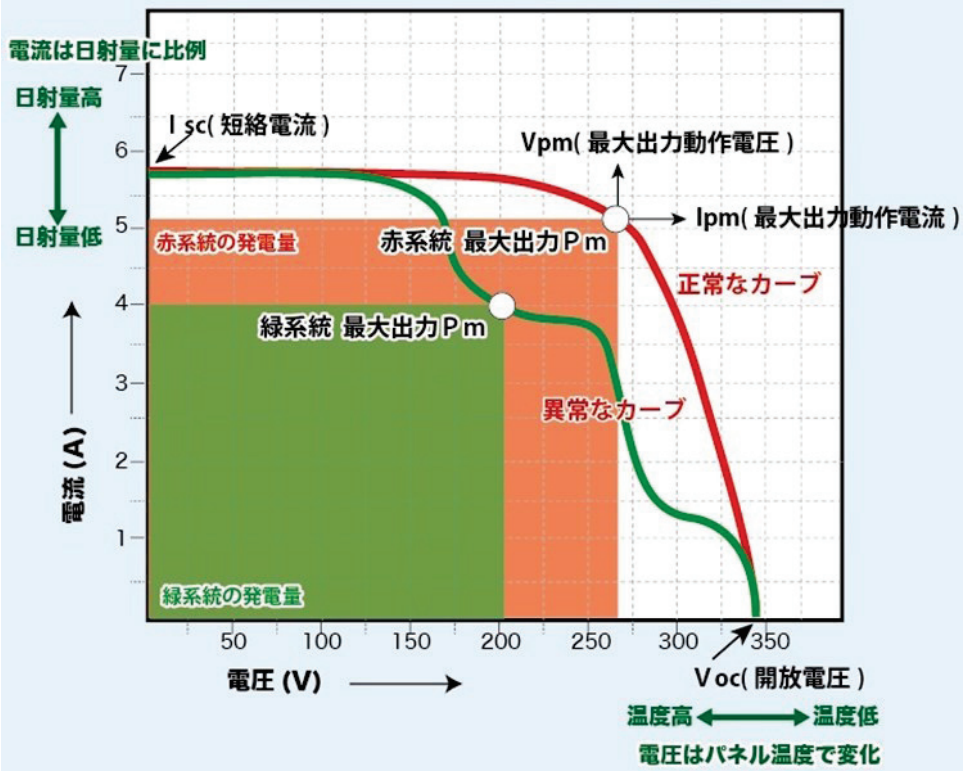

Fig. 2.2 An example image of current-voltage curve

To compare and judge the performance of various PV cells under the same conditions, a standard test conditions (STC)(ISO/IEC 60904-3, 2008) is proposed, which involves cell temperature (25°C), solar irradiance (1,000 W/m^2) and solar spectrum (air mass 1.5). In order to control the standard test condition easily, the PV module performance testing is always performed indoors so far, and it use a solar simulator to substitute the sun. But, with the outspread of solar PV modules, the needs for PV panel performance characterizations are required more than before not only for new type of PV panels but also for ones already installed. Recently, outdoor measurement techniques for the characterizations are developing and are becoming popular (Hishikawa et al., 2016). Although the traditional indoor testing keeps a high accuracy of PV performance testing, fixed operation place is difficult to apply to the installations already installed. Moreover, many PV devices exhibit a poor performance in actual use conditions. The outdoor

performance makes it easier to understand the performance of the panel in filed environment, and they also have potential advantages such as lower cost, and availability of spectrum close to air mass 1.5. However, the many high-accuracy PV performance testing are performed indoors by using solar simulators, because outdoor PV performance testing is affected easily by surrounding environments such as operating cell temperatures, and solar irradiances (Malik et al., 2003), so that there are not many opportunities to obtain precise PV performance testing. Therefore, outdoor testing is difficult to make sure the accuracy and repeatability of I-V curve measurement. In order to make a standard which determined the condition for precise outdoor PV performance testing, many investigations are conducted.

An investigation by the Photovoltaic Reliability Laboratory of Arizona State University indicated that the precise outdoor testing can be realized repeatedly under the following conditions: under clear sunny days (>90% direct normal irradiance), at lower air mass values (<2.5), using a fast (<1 s) I-V curve tracer, and pre-cooling of a test module to control the module temperature (Paghasian et al.2011). Other studies have pointed out the possibility of that precise outdoor testing under unstable weather conditions when the testing is performed within 0.1-0.2 s with a fast I-V meter (Hishikawa et al., 2015; Fukabori et al., 2015; Hishikawa et al., 2014). Nonetheless, for general weather conditions, the repeatability of the precise outdoor testing has not been explained definitely. As the major source of uncertainty related to outdoor PV module performance testing, quantitative analysis of solar irradiance fluctuations is required.

Usually, the fluctuations of solar irradiance in short period is mainly caused by clouds distribution and their movement. In Japan, the weather conditions change frequently and

clear-sky days are only 8% in a year, and therefore, the irradiance fluctuations occurred frequently in Japan. The outdoor performance testing has to conduct in cloudy day in Japan. It is significant to clear the characterization of solar irradiance fluctuations and find a method for selecting stable solar irradiance conditions for outdoor performance testing. Therefore, in this study, we employed several high speed pyranometers and a sky camera to characterize and quantify the fluctuations of solar irradiance in a short period and to find a method which can detect a stable weather conditions, especially a stable solar irradiance condition, for precise outdoor PV performance module testing.

2.2 Observation system

The observation system employed in this study mainly consists of several PV module sensors (PVMSs), a sky camera, and a series of accessorial observation devices include a short-wave radiometer, a long-wave radiometer and a weather station. They are located on the roof of engineering school of Gifu University, Japan (136°44’22”E, 35°22’51”). The observation system started working in March 2016 and has continued up to now. The overview of observation system is shown in Fig. 2.3, and the explanations in detail will be given at the next.

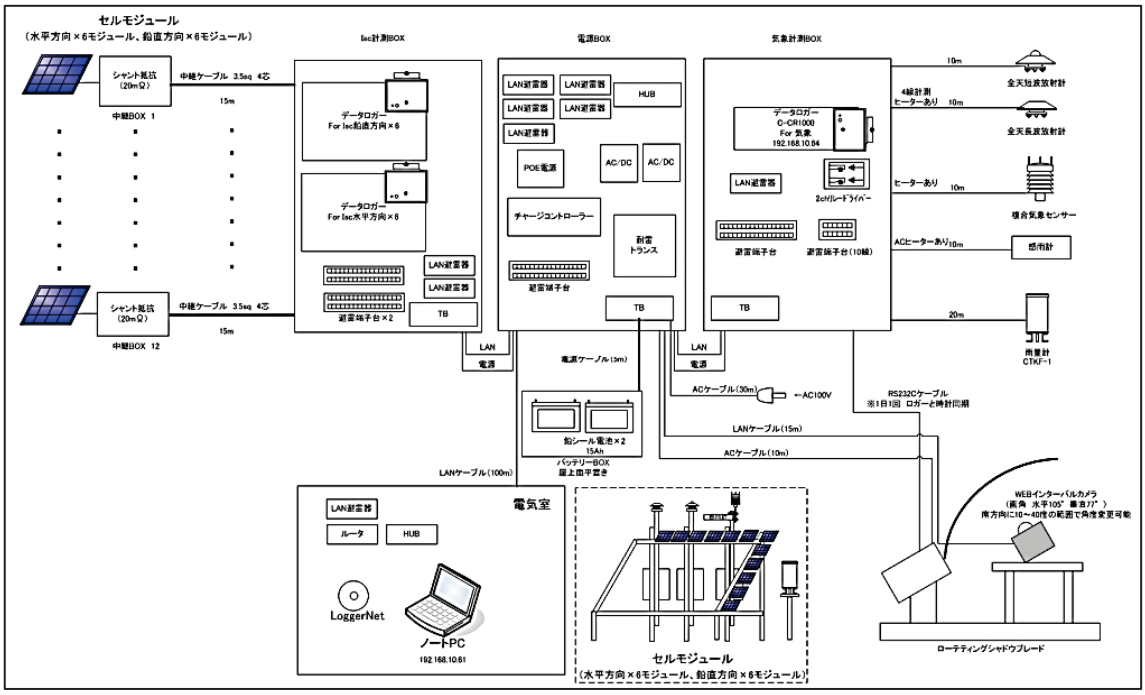

Fig. 2.3 Overview of observation system

2.2.1 PV module sensor

The PVMSs are conventional crystalline silicon (c-Si) PV modules (KISGT101F8D/AIST) and used as high-speed pyranometer for measuring the global irradiance. The structure of PVMS is shown in Fig. 2.4, it includes an active 5-inch c-Si cell and eight dummy cells surrounding it and named as PV module irradiance sensor. All the PVMSs have been calibrated at standard test conditions by indoor precision measurements (Hishikawa et al., 2016). As shown in Fig. 2.5, PVMSs are mounted on the rims of an existing PV panel rack facing to the south at 20.5° tilted angle. Six PVMSs are arranged in a straight line from west (No.1) to east (No.6) and the others are arranged from the south (No.1) to the north (No.6). The distance between neighboring PVMSs is 1.145 m. They measure solar irradiance at 10 ms sampling intervals. Temporal variation of solar irradiance is measured with each PVMS, and spatial variation is evaluated as the instantaneous irradiances observed with a set of PVMSs.

Therefore, the temporal and spatial fluctuations of solar irradiance can be observed simultaneously. An example of time series of solar irradiance observed by the PVMSs in west-east direction and south-north direction is shown in Fig. 2.6. The solar irradiance time series draw sinusoidal curves according to the altitude of sun. And the solar irradiance fluctuated frequently due to the moving of cloud. The fluctuations of solar irradiance caused by cloud movement are measured continuously from 6:00:00 to 18:00:00. There are similar patterns of time series of solar irradiance observed in both west-east and south-north direction due to the closed distance between them.

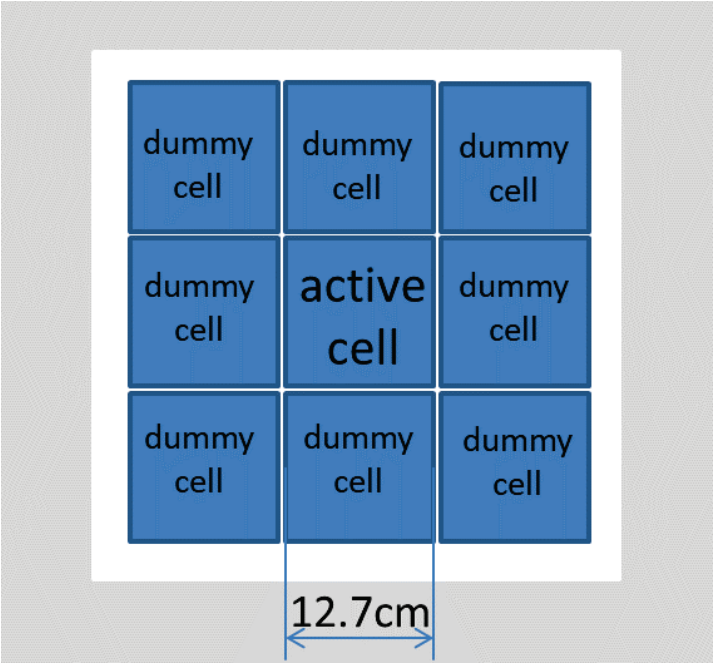

Fig. 2.4 The structure of PVMS

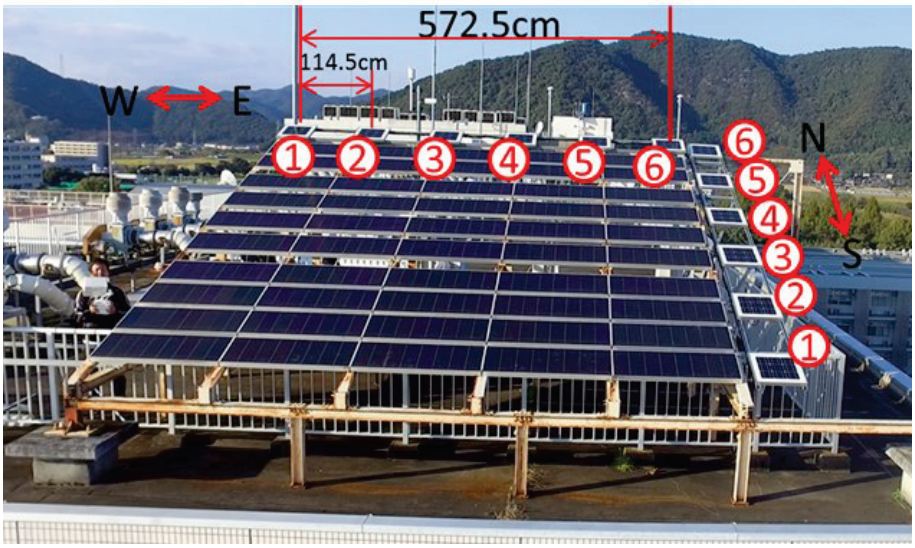

Fig. 2.5 Overview of PVMS

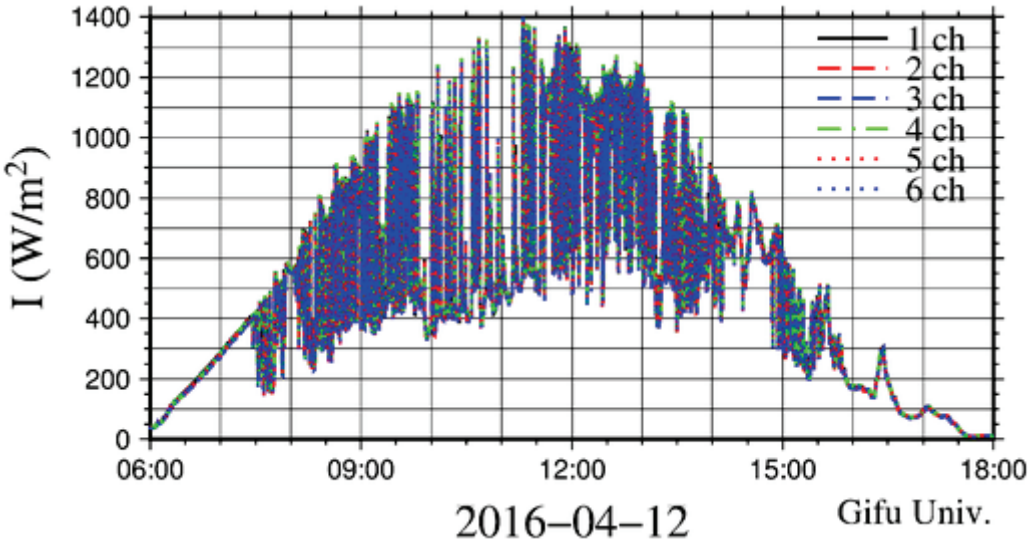

(a)

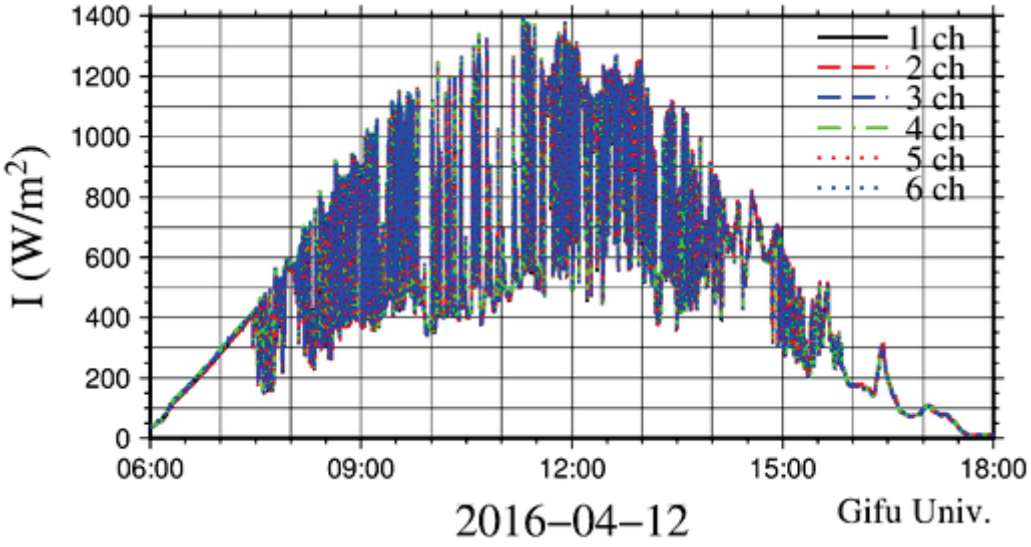

(b)

Fig. 2.6 Time series of solar irradiances observed with PVMSs

(April 12, 2016, (a).In west-east, (b).In south-north)

2.2.2 Sky camera

The sky camera (a fish-eye camera, Climatec CMT-S15D-D20-6MP) shown in Fig. 2.7 is used to monitor weather conditions and the distribution and deformation of clouds. The time interval of frames was 1 min from the start of experiments until April 11th, 2017, and later it was 15 s. A shadow blade is installed in front of the lens and its shadow moves as it follows the sun. It shades the direct solar irradiance into the lens, and only clouds near the sun can be photographed with its support (Zhang et al., 2017). Figure 2.8 shows the cloud image monitored by the sky camera and the sun is shaded by the black blade.

Fig. 2.7 Sky camera with shadow blade

Fig. 2.8 Cloud distribution observed with sky camera (April 17, 2016 12:00:00)

2.2.3 Other monitor devices

There are some other monitor devices installed on the rims of rack near PVMSs. As shown in Fig. 2.9, a conventional short-wave pyranometer (Climatec CHF-L02P, Fig. 2.10) is installed for reference of PVMSs. A large-wave radiometer (Climatec CHF-IR02, Fig. 2.11) is introduced in this study for measuring the parameter of cloud bottom height. So we can evaluate the height of clouds. A weather station device also has been set to monitor the weather conditions around observation site such as air temperature, wind speed and wind direction, humidity and other meteorological factors as shown in Table 2.1.

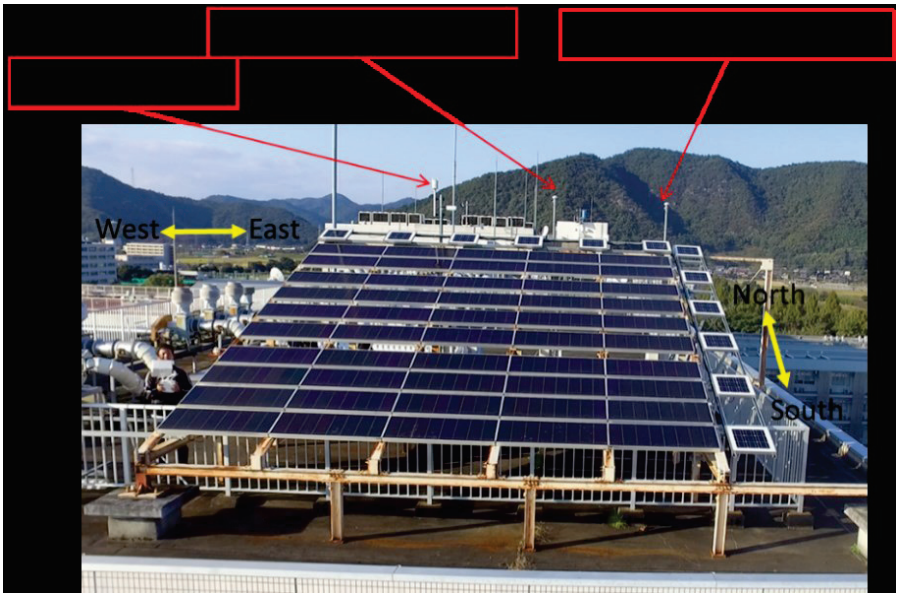

Fig. 2.9 Weather station, long-wave and short-wave monitor devices

Fig. 2.10 Short-wave radiometer CHF-L02P

Fig. 2.11 Long-wave radiometer CHF-IR02

Table 2.1 The output data and measurement range observed by weather station device

Items	Wind		Temperature (°C)	Humidity	Atmospheric pressure (hPa)	Precipitation intensity (mm/h)
	Speed (m/s)	Direction (°)				
Measurement range	0~60	0~360	-52~＋60	0~100％ RH	600~1100	0~200

Reference

1. Photovoltaic Devices, (2008). Part 3: Measurement Principles for Terrestrial Photovoltaic (PV) Solar DevicesWith Reference Spectral IrradianceData,IEC 60904-3.
2. Hishikawa, Y., Doi, T., Higa, M., Yamagoe, K., and Ohshima, H., (2016). Precise Outdoor PV Module Performance Characterization Under Unstable Irradiance, IEEE Jour. Photovoltaics, Vol. 6, No. 5, pp.1221-1227.
3. Malik, A.Q., Damit, S.J.B.H., (2003). Outdoor testing of single crystal silicon solar cells. Renewable Energy, 28.9: 1433-1445.
4. Paghasian, K., and TamizhMani, G., (2011). "Photovoltaic module power rating per IEC 61853–1: A study under natural sunlight," Solar ABC Study Report, [Online].
5. Hishikawa, Y., Yamagoe, K., Ohshima, H., Tsuno, Y., and Kojima, H., (2015). "New technology for precise outdoor PV module performance measurements," in Proc. IEEE 42nd Photovolt. Specialist Conf., New Orleans, LA, USA, pp. 1–6.
6. Fukabori, A., Takenouchi, T., Matsuda, Y., Tsuno, Y., and Hishikawa, Y., (2015). "Study of highly precise outdoor characterization technique for photovoltaic modules in terms of reproducibility," Jpn. J. Appl.Phys., vol. 54, 08KG06.
7. Hishikawa, Y., Fukabori, A., Takenouchi, T., and Tsuno, Y., (2014). "Accurate outdoor measurement technology of PV devices," (in Japanese) in Proc. JSES JWEA Joint Conf., Fukushima, Japan, pp. 289–292.
8. Hishikawa, Y., Doi, T., Higa, M., Yamagoe, K., and Ohshima, H., (2016). Precise Outdoor PV Module Performance Characterization Under Unstable Irradiance,

IEEE Jour. Photovoltaics, Vol. 6, No. 5, pp.1221-1227.

9. Zhang, J.F., Watanabe, K., Kobayashi, T., Yoshino, J., (2017). Analysis of Solar Irradiance Sudden Changing for PV Panel Outdoor Testing. IEEJ,7-024, 2017.

Chapter 3 Short-period fluctuations of solar irradiance and cloud conditions

3.1 Introduction

In recent years, the topic of solar irradiance fluctuations has been discussed in a large number of literatures and a substantial amount of works in order to understand the nature of the variability of solar irradiance. But most of these aim to evaluate the relationship between solar irradiance fluctuations and PV power fluctuations. So the target area and time period are often set very wide. For example, Otani and coworkers (1997) investigated the relationship between solar irradiance fluctuations and the total panel area of a PV system, and proposed the optimum size of the total panel area for reducing fluctuations on PV output. They also defined the fluctuation factor to evaluate the fluctuations qualitatively, and calculated power spectra of the irradiances for analyzing characteristics of solar irradiance fluctuations. The methods how to eliminate the effects of solar irradiance fluctuations on PV grid fluctuations also have been discussed by these researchers. For example, David et al. (2014) observed PV output from 13 stations in a small insular grid, and analyzed the temporal and spatial fluctuations of PV output from individual stations and each station-pair with different distances. They also discussed spatial smoothing effect by comparison of fluctuations between individual station output and averaged output of stations surrounding it. Murata et al. applied the same analysis as David et al. (2014) by using observed data from 52 PV stations across Japan, and discussed geographical smoothing effect by grouping stations. For the PV module performance characterizations, the fluctuation of solar irradiance should be discussed in second-time and module level, so the target range in time is less than 1 s

and in space is 1 to 10 meters. In this chapter, we analyzed the characterization of solar irradiance fluctuation in short-period of 1 s and cloud conditions.

3.2 The analysis of change rate of solar irradiance in 1 s.

As described earlier, the high-speed measurement of I-V meters are necessary for outdoor PV module performance testing with appropriate high accuracy. The proposed measuring interval is 1 s in USA (Paghasian et al., 2011) and 0.2 s in Japan (Hishikawa et al., 2014; Fukabori et al., 2015; Hishikawa et al., 2015) as explained before. In this study, the characteristic of short-period solar irradiance fluctuations within 1 s is discussed. The datasets are selected for one year, from 6 March 2016 to 31 March, 2017. In order to avoid the effect from low solar incident angle, the target period is from 9:00:00 to 15:00:00 in this study.

The change rate of solar irradiance in 1 s was used as the index of the characterization of short-period irradiance fluctuations. Clear-sky index CI, which is the irradiance normalized by the clear sky global solar irradiance, is calculated for avoiding the effect of solar altitude. The rate of change of solar irradiance in 1 s is calculated by the following equation.

$$\text{Rate of change of solar irradiance} = \frac{CI_{after} - CI_{before}}{\Delta t} \qquad (3\text{-}1)$$

Where, Δt is the time interval and $\Delta t = 1s$, CI_{after} and CI_{before} are clear-sky indices after and before measuring the time interval. This parameter corresponds to changing speed of solar irradiance as shown in Eq. (3-1). The occurrence frequency of the solar irradiance change rate in 1 s in each month is shown in Fig. 3.1. In this figure, the data concentrates just around zero in change rate, meaning that events with small change in the interval, 1 s, are dominant. The difference of occurrence frequency between each month

was indicated in this figure, however the difference seems small. The cumulative occurrence frequency of the solar irradiance change rate in 1 s is shown in Fig. 3.2(a), and the enlarged figure of its part is shown in Fig. 3.2(b). It can also be found that most events concentrate around zero in the rate of change. Differences of the change rates between each month can be found in Fig. 3.2, especially in Fig. 3.2(b). The fluctuations of solar irradiance in autumn (indicated with yellow lines in the figure) and winter (blue lines) are larger than others in the figure. This monthly difference may be caused by the weather characteristics, e.g. unstable or not, cumulus clouds or stratus clouds etc., in each month. For discussion about averaged monthly or seasonal characteristics in irradiance change rate, several-years continuous observation should be required.

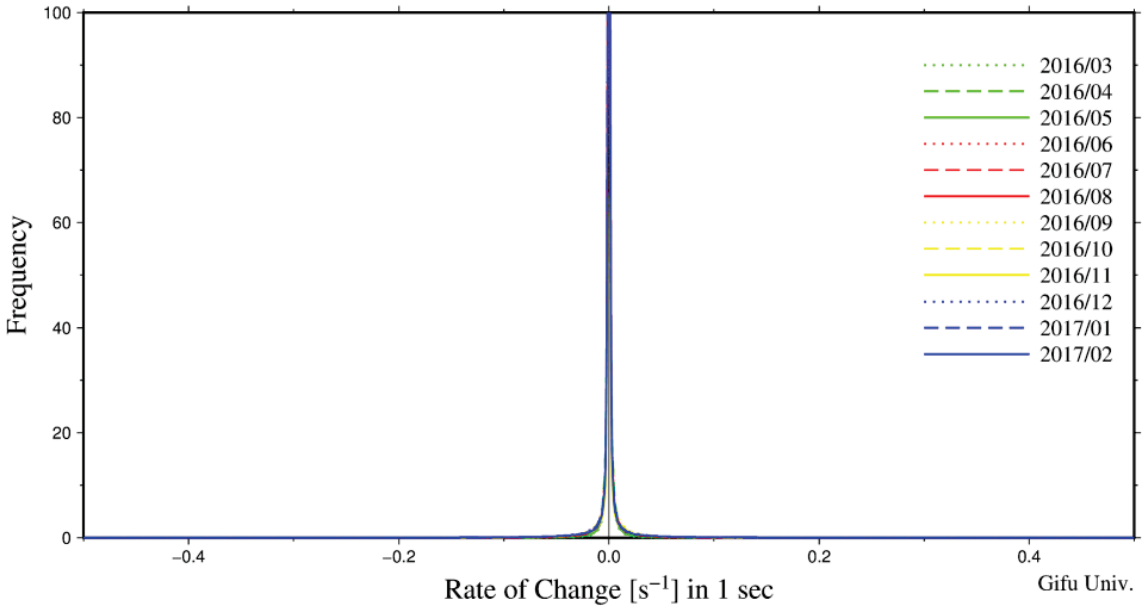

Fig. 3.1 The distribution of occurrence frequency for solar irradiance change rate in 1 s.

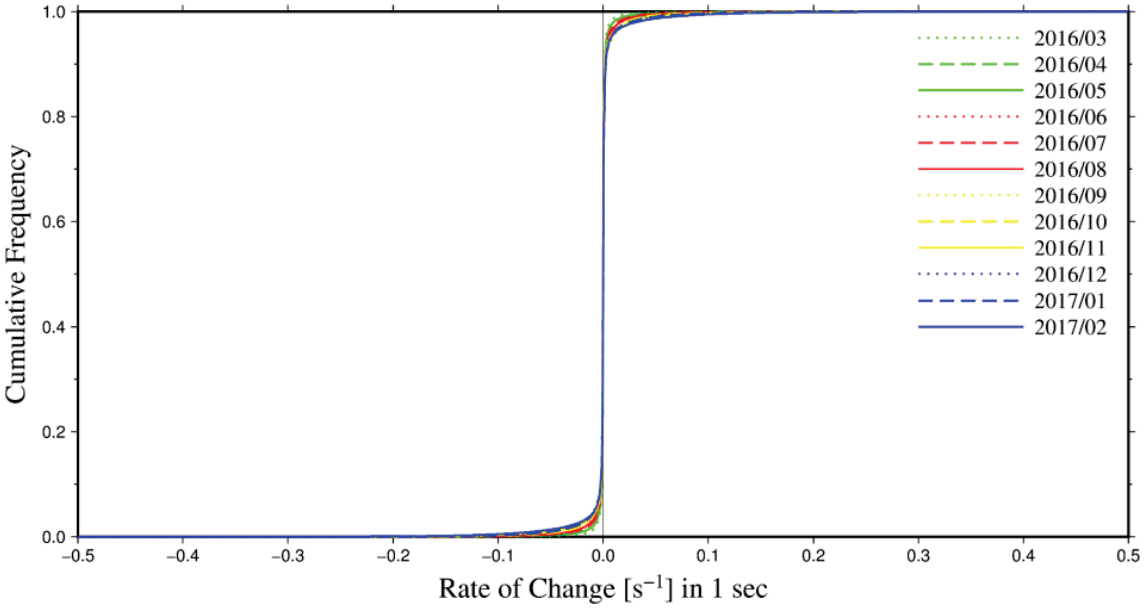

(a)

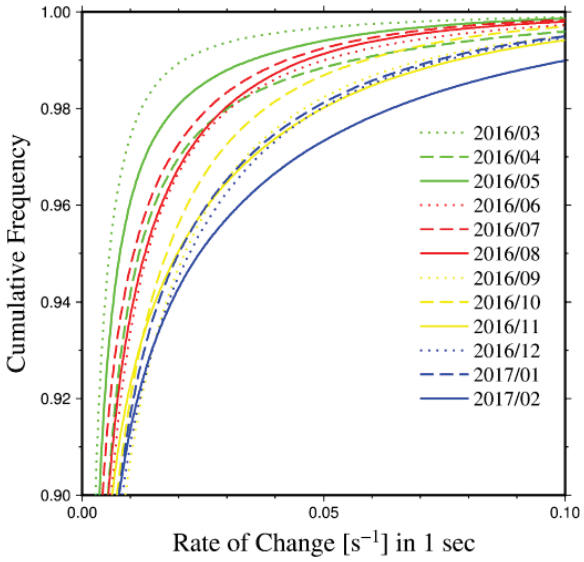

(b)

Fig. 3.2 The cumulative frequency of the solar irradiance change rate in 1 s (a) and the enlarge figure around change rate 0 which range of cumulative frequency is from 0.90 to 1.00 (b).

Table 3.1 Change rate of solar irradiation intensities and its coverage rate of cumulative frequency distribution.

Change rate of solar irradiation intensities in 1 s	1σ (0.013389)	2σ (0.026778)	3σ (0.040167)
Coverage rate of cumulative frequency distribution	94.7%	97.1%	98.2%

The standard deviation of the change rate in 1 s of solar irradiance has been calculated from the available data. The change rate of solar irradiance intensities and its coverage rate of cumulative frequency distribution are indicated in Table 3.1. It can be found that in 94.7% of the observation period, the change rate in 1 s is less than 1.0%. This means the events with small irradiance fluctuations, which are required for the outdoor testing of PV modules, can be found easily under Japanese weather

3.3 Sudden changing of solar irradiance and weather conditions

Sudden changing of solar irradiance is predominantly caused by moving clouds. The changes are detected with the PVMSs and are discussed here in this study, along with cloud conditions observed with the sky camera here in this study. Figure 3.3 shows the solar irradiance time series on April 17, 2016, when the irradiance fluctuation is severe. The daily solar irradiance changed from low-irradiance and low-fluctuation in the morning to high-irradiance and low-fluctuation in the late afternoon through the period with extreme fluctuations in the early afternoon, as shown in the figure. The weather in the morning and in the late afternoon was thickly cloudy and cloudless, respectively. A cloud image taken by the sky camera is also indicated in Fig. 3.4 when the extreme

fluctuations occurred in the early afternoon. In this figure, the sun is behind the shadow-blade. The largest change rate of the irradiance is -63.4%/s, and it is the largest solar irradiance fluctuation throughout the study period. From the analysis of the cloud images, large fluctuations tend to occur when the cumuliform clouds with thick edges pass in front of the sun. According to the statistical analysis, large fluctuation events with a change rate of more than 0.6, like the event in Fig. 3.3, occur once at every couple of months.

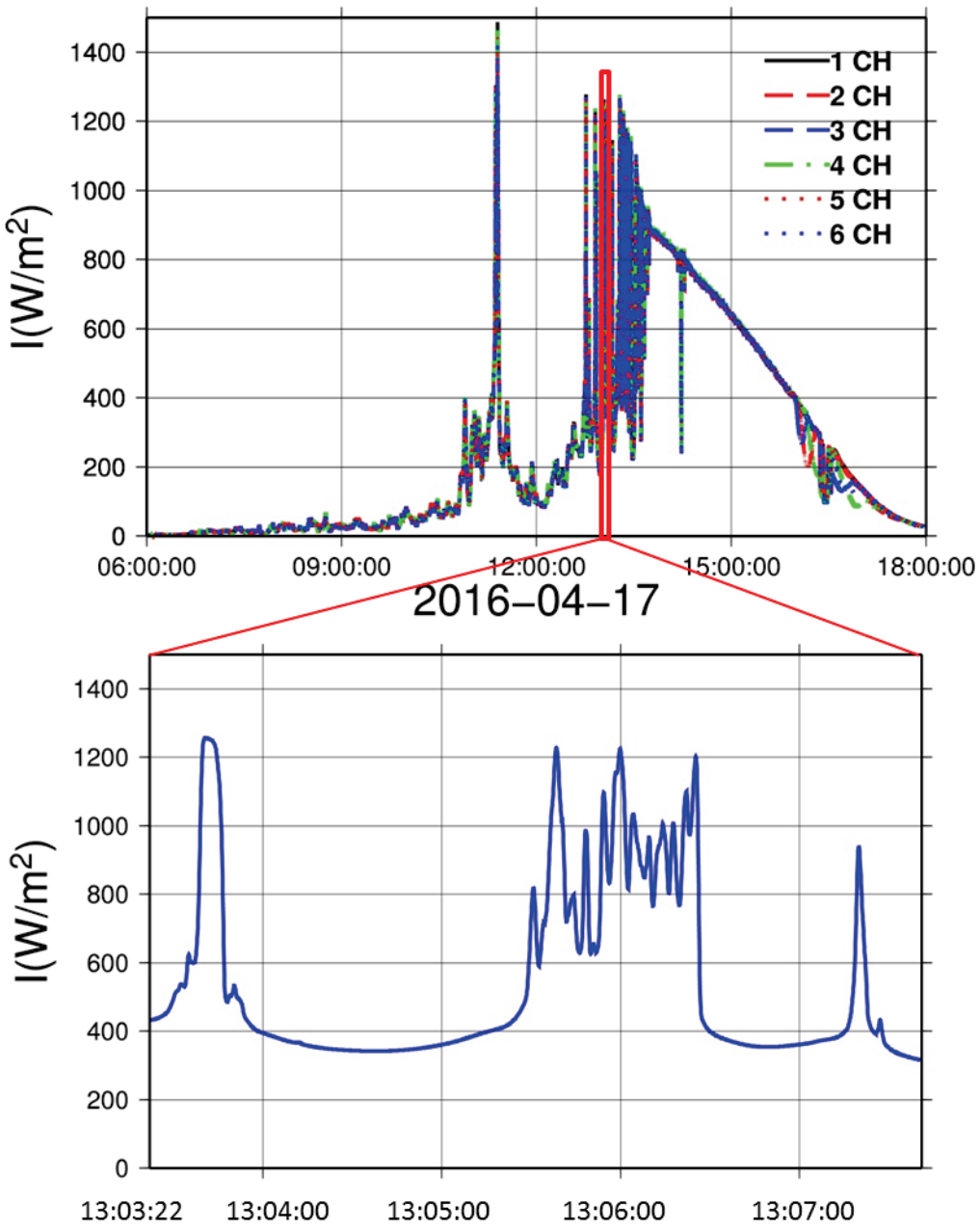

Fig. 3.3 An example of time series solar irradiance intensity (April 17, 2016, Gifu University)

Fig. 3.4 Cloud image when solar irradiance changed suddenly; Taken by sky camera, the black band in it is the shadow blade. (April 17, 2016. 13:07)

3.4 Summary

Solar irradiance and weather conditions are observed with PV module sensors (PVMS) and a sky camera, respectively, and short-period fluctuations of solar irradiance and the corresponding cloud conditions have been analyzed and discussed in this study. This observation and analysis are for the appropriate weather conditions for the outdoor PV module performance characterizations. From the observation data in one year, it is found that the change rate of clear-sky index in 1 s is less than 1.0% in 94.7% of the observation period under Japanese weather conditions. It follows that the stable irradiance conditions for the outdoor testing can be found easily under Japanese weather. On the other hand, the events with large fluctuations also were observed under the cumuliform cloud conditions, but the occurrence is low. It is also suggested that large fluctuations of the irradiance tend to occur when cumuliform clouds with thick edges pass in front of the sun.

Reference

1. Otani, K., Minowa, J., and Kurokawa, K., (1997). Study on areal solar irradiance for analyzing areally-totalized PV systems. Solar Energy Materials and Solar Cells, 47(1-4), 281-288.
2. David, M., Andriamasomanana, F. H. R., and Liandrat, O., (2014). Spatial and temporal variability of PV output in an insular grid: Case of Reunion Island. Energy Procedia, 57, 1275-1282.
3. Paghasian, K., and TamizhMani, G., (2011). "Photovoltaic module power rating per IEC 61853–1: A study under natural sunlight," Solar ABC Study Report.
4. Hishikawa, Y., Yamagoe, K., Ohshima, H., Tsuno, Y., and Kojima, H., (2015). "New technology for precise outdoor PV module performance measurements," in Proc. IEEE 42nd Photovolt. Specialist Conf., New Orleans, LA, USA, pp. 1–6.
5. Fukabori, A., Takenouchi, T., Matsuda, Y., Tsuno, Y., and Hishikawa, Y., (2015). "Study of highly precise outdoor characterization technique for photovoltaic modules in terms of reproducibility," Jpn. J. Appl.Phys., vol. 54, 08KG06.
6. Hishikawa, Y., Fukabori, A., Takenouchi, T., and Tsuno, Y., (2014). "Accurate outdoor measurement technology of PV devices," (in Japanese) in Proc. JSES JWEA Joint Conf., Fukushima, Japan, pp. 289–292.

Chapter 4 Short-period fluctuation and spatial distribution of solar irradiance under clouds

4.1 Introduction

In most cases, the irradiance fluctuations in a short time are caused by cloud distributions and their behavior. Many investigations and analyses about solar irradiance fluctuations due to cloud distributions and movements have been carried out. Their time scales range very widely, from long-timescale ranging from months to years to short-timescale ranging from milliseconds to days. Various parameters, such as variability index, clear-sky index and fluctuation factor have been introduced in order to understand solar irradiance fluctuations under clouds. For example, Tomson et al.(2006) calculated 10-minute absolute sums of irradiance observed with 1 minute intervals, and distinguished events in which sums exceed 1000 W/m^2, as unstable ones. They also derived linear functions on logarithmic axes for the relationship between changing rates of irradiance within 1 minute and their incidence in the events. On the other hand, spatial variations of solar irradiance have also been studied by observations at several different stations or PV plants (Otani et al., 1997; Barnett et al., 1998; Lave et al., 2010; Kariuki et al., 2018; Perez et al., 2012; Hoff et al., 2012; Tripathy et al., 2017). The purpose of the studies is mainly the understanding of correlations of irradiance fluctuations between PV plants caused by cloud distributions and their behaviors, and furthermore reducing the fluctuation of electric power generated by large PV plants consisting of several plants. Therefore spatial scale of the studies above corresponds to PV plants or distance between plants.

In this study, the time and space variations of solar irradiance are discussed for outdoor

PV module performance characterizations, therefore the target spatial scale corresponds to a module-size of several meters, and accordingly the temporal scale may be several seconds or less. Studies about such small spatial and temporal scale fluctuations of solar irradiance are limited. In these scales, irradiance fluctuations may be induced by an individual cloud and its movement, and cloud type may also affect the characteristics of the fluctuations. Therefore, in the present study, solar irradiance is observed with a series of high-speed pyranometers, and temporal instability and spatial nonuniformity of solar irradiance in short-period are discussed, including the effect of cloud type. Additionally, the travelling of clouds which also causes the fluctuations is discussed in this paper.

4.2 Cloud shadow movement caused by cloud advection.

Cloud shadows move on the ground as the clouds move. In the observation system, PVMSs are arranged in two lines in west-east and south-north directions; therefore, the movement of cloud shadows can be detected as the delay of irradiance fluctuations between PVMSs. Figure 4.1 shows the time series of solar irradiance observed with PVMSs at around 12:57:05 on April, 13, 2017. In the figure, delay between PVMSs with the same irradiance intensity corresponds to the elapse time of cloud shadow movement between them, and the instantaneous difference in irradiance intensity between them corresponds to the spatial nonuniformity of the irradiance. The distance between both PVMS No. 1 (W 1) and No. 6 (W 6) in the west-east line and between No. 1 (S 1) and No. 6 (S 6) in the south-north line is 5.725 m, and the delays of irradiance fluctuation are 200 and 500 ms, respectively, as shown in Fig. 4.1. If we assume that the deformation of clouds can be ignored, the speed of cloud shadow movement can be calculated on the basis of delays and distances between PVMSs. The speeds of a moving cloud are estimated as 28.6 m/s from east to west and 11.5 m/s from south to

north, as shown in Table 4.1. From these data, the speed and direction of the moving cloud are 30.8 m/s and 112° (east-south-east) in nautical convention, which is the direction where the wind comes from, measured clockwise from the geographic north. Wind speed and direction observed on the ground are also shown in the table as a reference. The speed of moving cloud shadows, i.e., the speed of the movement of clouds themselves, is usually higher than the wind speed on the ground, because wind speed at the upper atmosphere is usually higher than that on the ground. The wind direction observed on the ground towards the east-south-east is almost the same as the direction of moving cloud shadows.

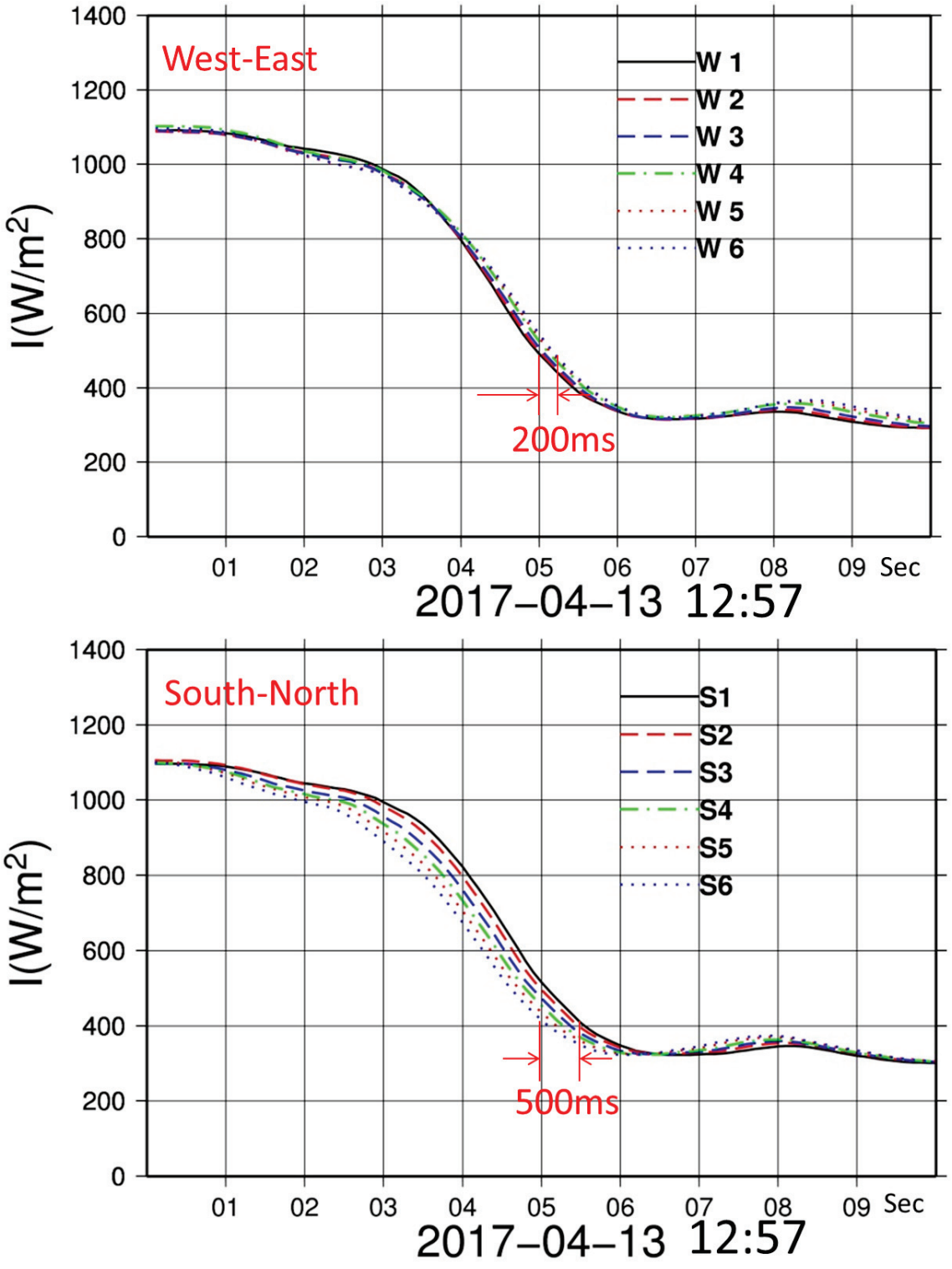

Fig. 4.1 Time series of solar irradiance intensities observed with PVMSs

(April 13, 2017 12:57:00 – 12:57:10)

Table 4.1 Evaluated moving speed of cloud and observed wind on ground (April 13, 2017 12:57:05)

Direction	Irradiance observed by PVMS W1 and W6,or S1and S6		
	Time delay (ms)	Distance between PVMSs (m)	Estimated cloud speed (m/s)
West-East	-200	5.725	-28.6
South-North	500	5.725	11.5

	Cloud speed (m/s)	Direction (Nautical convention)
Estimated from above result	30.8	112°(East-South-East)
Observed on ground	4.175	103°(East-South-East)

(a) (b)

Fig. 4.2 Cloud patterns obtained with sky camera at (a) 12:57:05, (b) 12:57:20 (April 13, 2017).

Figure 4.2 shows cloud images taken by the sky camera at the times 12:57:05 and 12:57:20 corresponding to the PVMS observation time in Fig. 4.1. The time interval between the images is 15 s. Clouds near the sun are moving in the same direction as those shown in Table 4.1 in the figure without deforming.

4.3 Temporal instability and spatial nonuniformity of solar irradiance under different weather conditions classified on the basis of cloud distributions

Temporal instability and spatial nonuniformity of solar irradiance can also be detected from PVMSs observation. The temporal instability of solar irradiance is described as the variation of the irradiance observed with a single PVMS. On the other hand, the spatial nonuniformity of solar irradiance corresponds to a difference in the instantaneous irradiance intensity between PVMSs, as explained in the previous section. The magnitude of spatial irradiance deviations depends on the weather conditions, especially cloud distributions or cloud types (Duchon et al., 1999). Japanese Meteorological Agency categorizes weather from cloud cover. It is indicated 10 ranks from 0 (no cloud) to 10 (completely covered with clouds). Rank 0 and 1 is called “Clear sky (no cloud)”, 2 to 8 is “Fine sky with clouds”, and 9 and 10 is “Cloudy sky”. Solar irradiances and cloud conditions observed in this study under the typical weathers are indicated in Fig. 4.3. As shown in the figure, the irradiance is stable in short period under clear sky. Under fine sky with clouds, the clouds are usually cumulus clouds, and the irradiance fluctuates evidently. Under cloudy sky, the clouds are usually stratus clouds, and the irradiance is weaker than the other weather conditions.

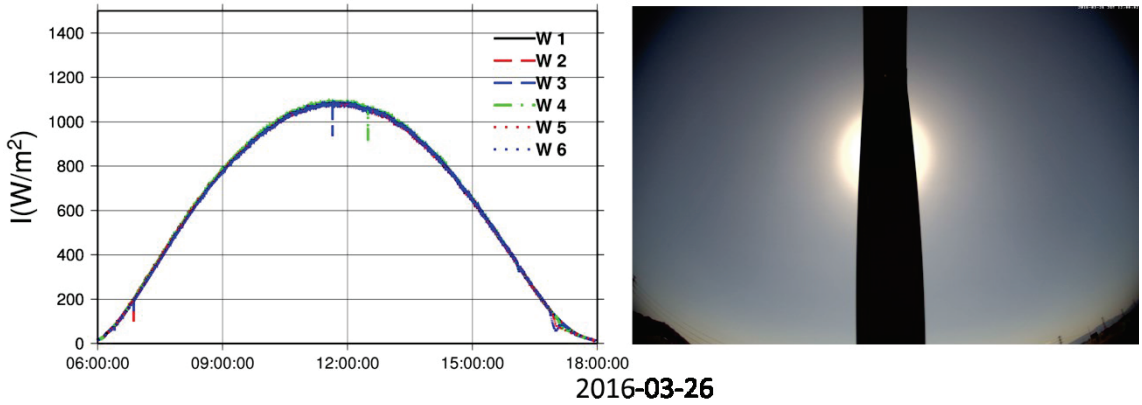

(a)

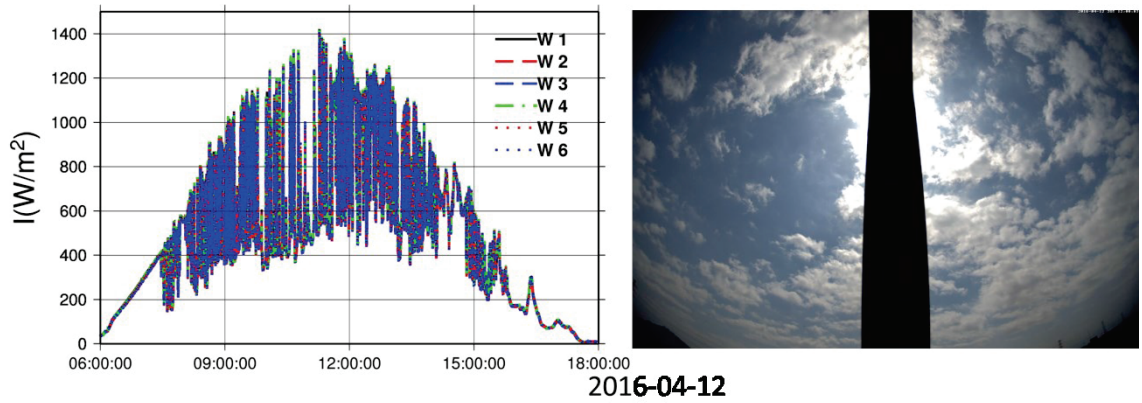

(b)

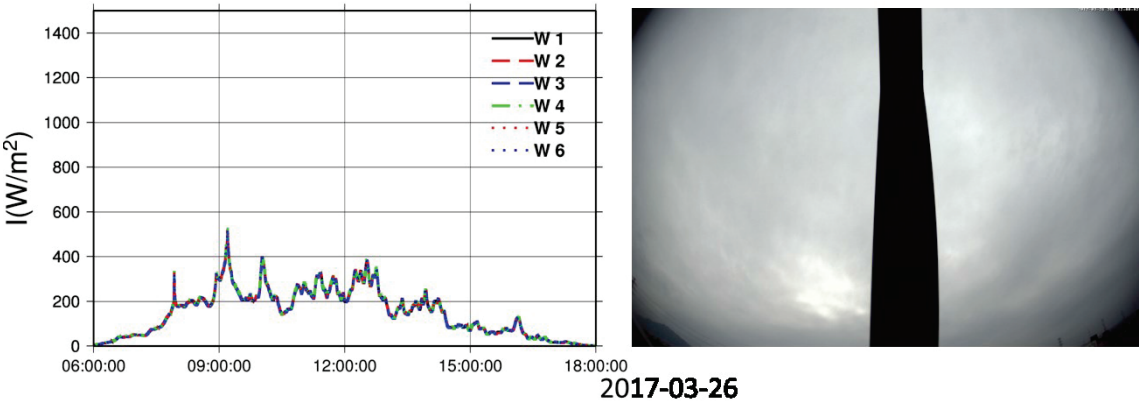

(c)

Fig. 4.3 Solar irradiances and cloud conditions observed under the typical weathers.

(a) Clear sky, (b) Fine sky with clouds, (c) Cloudy sky.

In Meteorology, clouds are classified into two major cloud types according to their visual appearance from the ground: cumulus clouds with vertical development, stratus clouds in flat-appearing layers and cirrus clouds with fibrous or smooth appearance (Sandra, 2011). Figure 4.4 shows occurrence frequency of weather conditions in the observation. The clear skies are observed only 8 % in the observation period. On the other hand, more than half of all days in the period are fine skies with clouds, under which weathers solar irradiances fluctuate in short period, therefore the weather divide into “fine sky with a few clouds” and “fine sky with numerous clouds”. From the discussion, weather conditions are classified into four types here: no clouds (clear sky), numerous clouds (fine sky with numerous clouds), a few clouds (fine sky with a few clouds), and completely-cover clouds (cloudy sky). The typical days under these weathers or clouds are selected and their characteristics of solar irradiance fluctuations are analyzed.

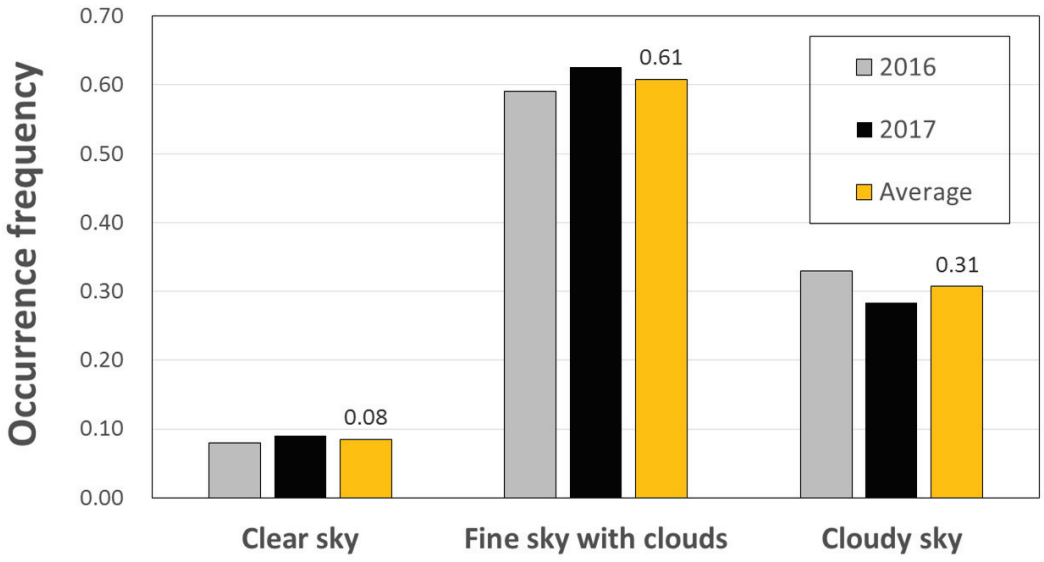

Fig. 4.4 Occurrence frequency of weather conditions in the observation.

4.3.1 No clouds (clear sky)

The day April 15, 2016 is selected as the typical day with a clear sky. Solar irradiance time series observed using west-east PVMSs daily and in a short period of 20 s at around 12:00:10 on a clear-sky day are shown in Fig. 4.5. The weather is clear during that day, and no clouds are found in the sky image taken with the sky camera as shown in Fig. 4.6. The solar irradiance time series draw sinusoidal curves according to the sun's altitude. The observed irradiance changes smoothly, and no short-period fluctuations are found. It is also clear that all the lines in Fig. 4.5 almost coincide. It means that no deviations of solar irradiance between PVMSs exist. The same characteristics are found in the solar irradiance time series observed with PVMSs in the south-north line. Therefore, no irradiance fluctuations in time and space exist on clear-sky days, and solar irradiance is stable

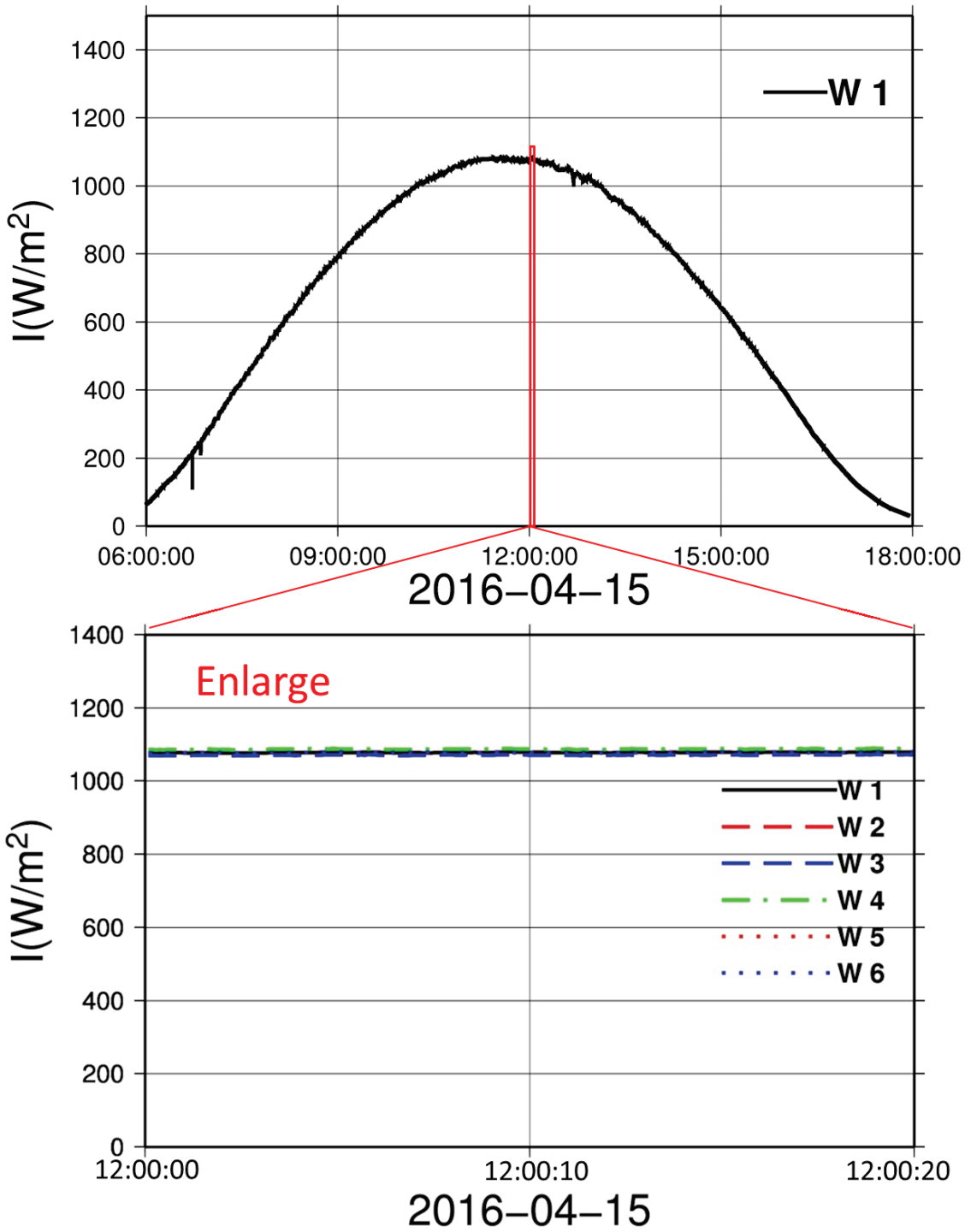

Fig. 4.5 Time series of solar irradiance in daily and short period (20s) in a clear-sky day

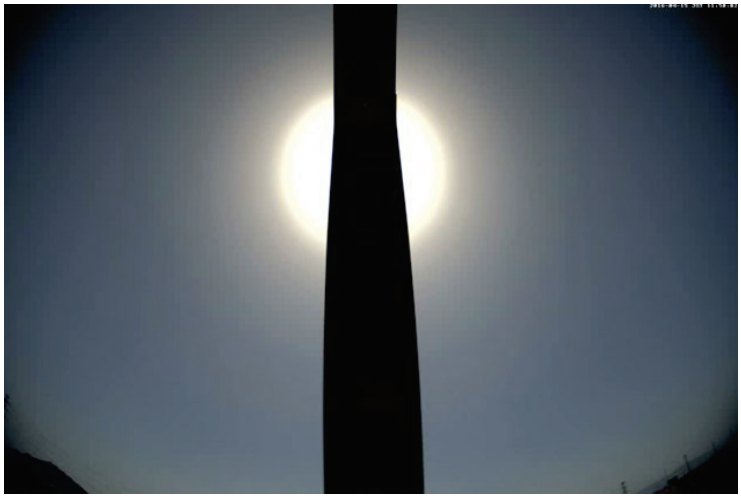

Fig. 4.6 Sky image taken by sky camera (April 15, 2016 12:00:00)

4.3.2 Numerous cumulus clouds (cloudy sky)

The day April 12, 2016 is selected as the typical day when numerous clouds cover the sky with gaps as shown in Fig. 4.7. The observed solar irradiance fluctuates markedly with time as shown in Fig. 4.8. Under this weather condition, the cloud type is usually cumulus. The fluctuations occur because the direct irradiance is blocked by clouds frequently. Not only daily solar irradiance time series observed using PVMSs in the west-east line, short-period solar irradiance is also indicated in Fig. 4.8. Large solar irradiance fluctuations, which correspond to the amplitude of irradiance fluctuations normalized by clear-day irradiance at noon, occur at a rate of 70% at around 11:30. The difference in instantaneous irradiance between different PVMSs can also be found evidently while the irradiance changes rapidly as shown in Fig. 4.8. In the figure, the irradiance observed with each PVMS varies, as determined by following that observed with PVMS NO.1 with the same track patterns. It means that the cloud edge moved from upstream (west, No.1) to downstream (east, No.6); therefore, the PVMSs measure

the moving shadows of the clouds running from the west to the east. The large difference in instantaneous irradiance between PVMS No. 1 and PVMS No. 6 is determined as 130 W/m^2 at 11:28:11 on the target day. As the distance between PVMSs (5.725 m) and clear-day irradiance at noon (1,260 W/m^2), the averaged spatial nonuniformity of irradiance can be calculated as 1.8%/m. By applying a similar analysis used in the previous section, the speed and direction of the cloud shadow moving over PVMSs are evaluated as 12.1 m/s and south-south-west, respectively.

Fig. 4.7 Cloud image observed with a sky camera (April 12, 2016 11:28:00)

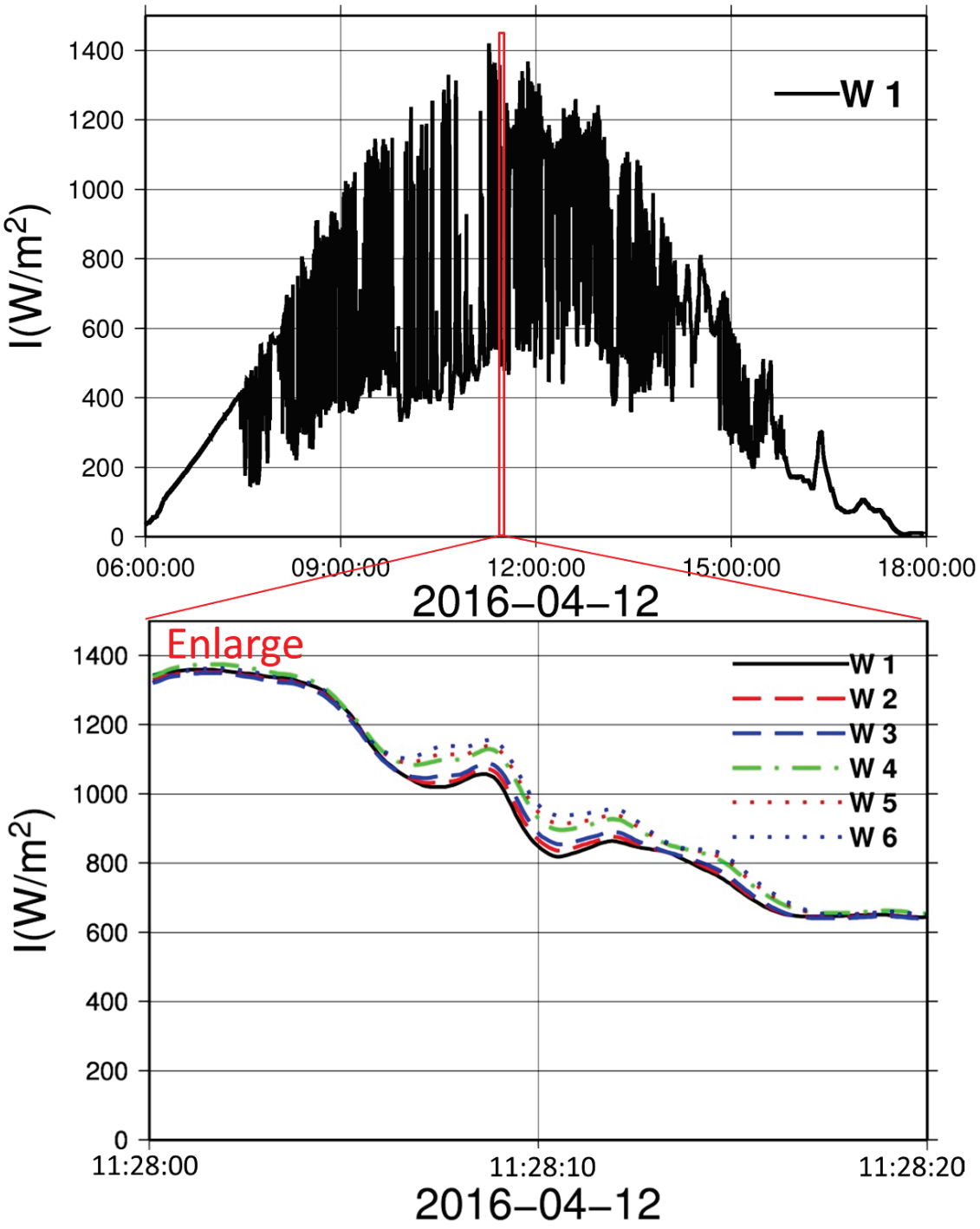

Fig. 4.8 Time series of solar irradiance in daily and short period (20s) in a cloudy day with numerous cumulous clouds

4.3.3 A few cumulus clouds (cloudy sky)

The day March 28, 2016 is selected as the typical day with a fine sky with a few clouds. Figure 4.9 shows a cloud image taken at 12:17:00 on the day that was cloudy with cumulus clouds distributed sparsely. The time series of solar irradiance observed using PVMSs in the west-east line for one day and in a short period at around 12:17:30 are shown in Fig. 4.10. Compared with Fig. 4.7, similar cumulus clouds are found in Fig. 4.9, but their coverage is low. The fluctuations of irradiance on this day are less frequent than those discussed in the previous section, and the maximum fluctuation is 72%, which is similar to that in Fig. 4.8. Similar to the previous section, the difference in instantaneous solar irradiance between different PVMSs is evident, as shown in Fig. 4.10, when the irradiance changes rapidly. From Figs. 4.8 and 4.10, the characteristics of events with rapid irradiance fluctuations are similar to those with cumulous clouds. Only the frequency of irradiance fluctuations is dependent on cloud coverage. The fluctuations of solar irradiance start from PVMS No. 1, and others occur after No. 1 in succession, so the clouds moved from the west (No. 1) to the east (No. 6). The PVMS measurements show that the shadows of the clouds are therefore moving from the west to the east. From the analyses carried out in the previous section, it is estimated that clouds over the target point move with a speed of 3.1 m/s, in the west-south-west direction. The maximum difference in the irradiance between PVMS No. 1 and PVMS No. 6 is about 91 W/m^2, which corresponds to 1.3%/m of clear-day irradiance at noon.

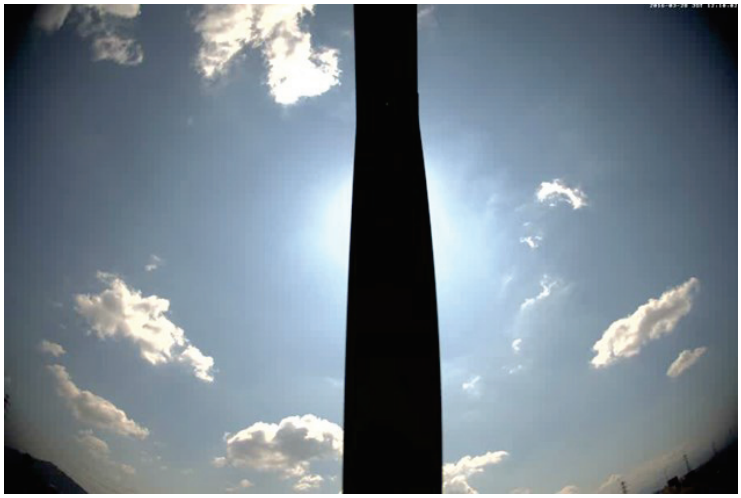

Fig. 4.9 Cloud image observed with sky camera. (March 28, 2016 12:17:00)

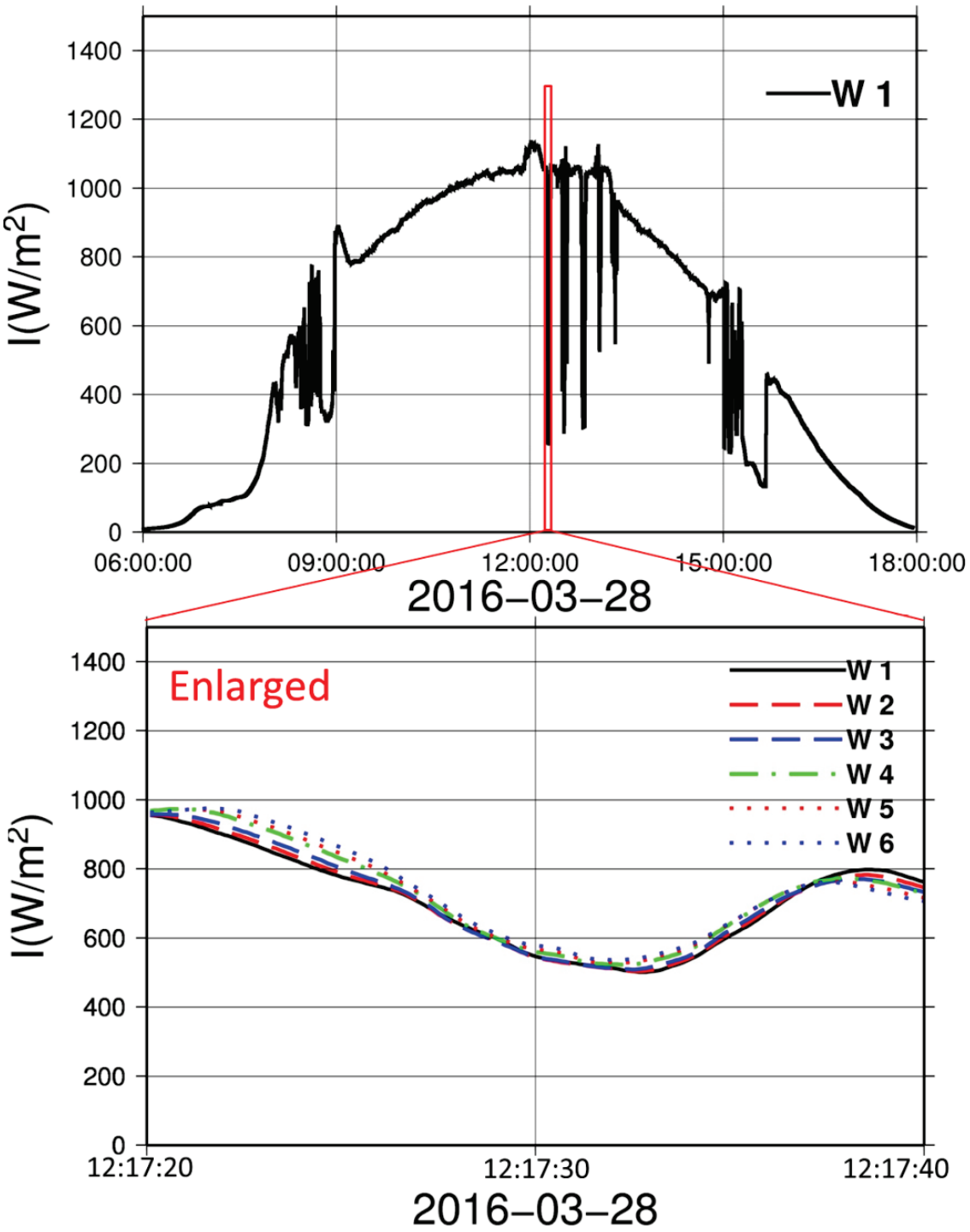

Fig. 4.10 Time series of solar irradiance in a day and in short period (20s) in a cloudy day with a few cumulous clouds

4.3.4 Stratus clouds (cloudy sky)

Figure 4.11 shows a typical cloudy day, April 5, 2016, with a cloudy sky. The whole sky is covered by layered clouds, and without any gaps. The fluctuations of solar irradiance for one day and in a short period at around 10:43:30 are shown in Fig. 4.12. In this figure, owing to cloud shading, the solar irradiance intensity is lower than those on other typical days discussed above. Solar irradiance fluctuations also exist with the maximum degree of 55%. However, the short-period fluctuations are relatively smaller, as shown in Fig. 4.12, than those under weather conditions with cumulous clouds shown in Figs. 4.8 and 4.10. It means that the irradiance under conditions with stratus clouds is relatively stable and uniform, similar to that with a clear sky shown in Fig. 4.5.

Fig. 4.11 Cloud image observed with sky camera (April 5, 2016 10:43:00)

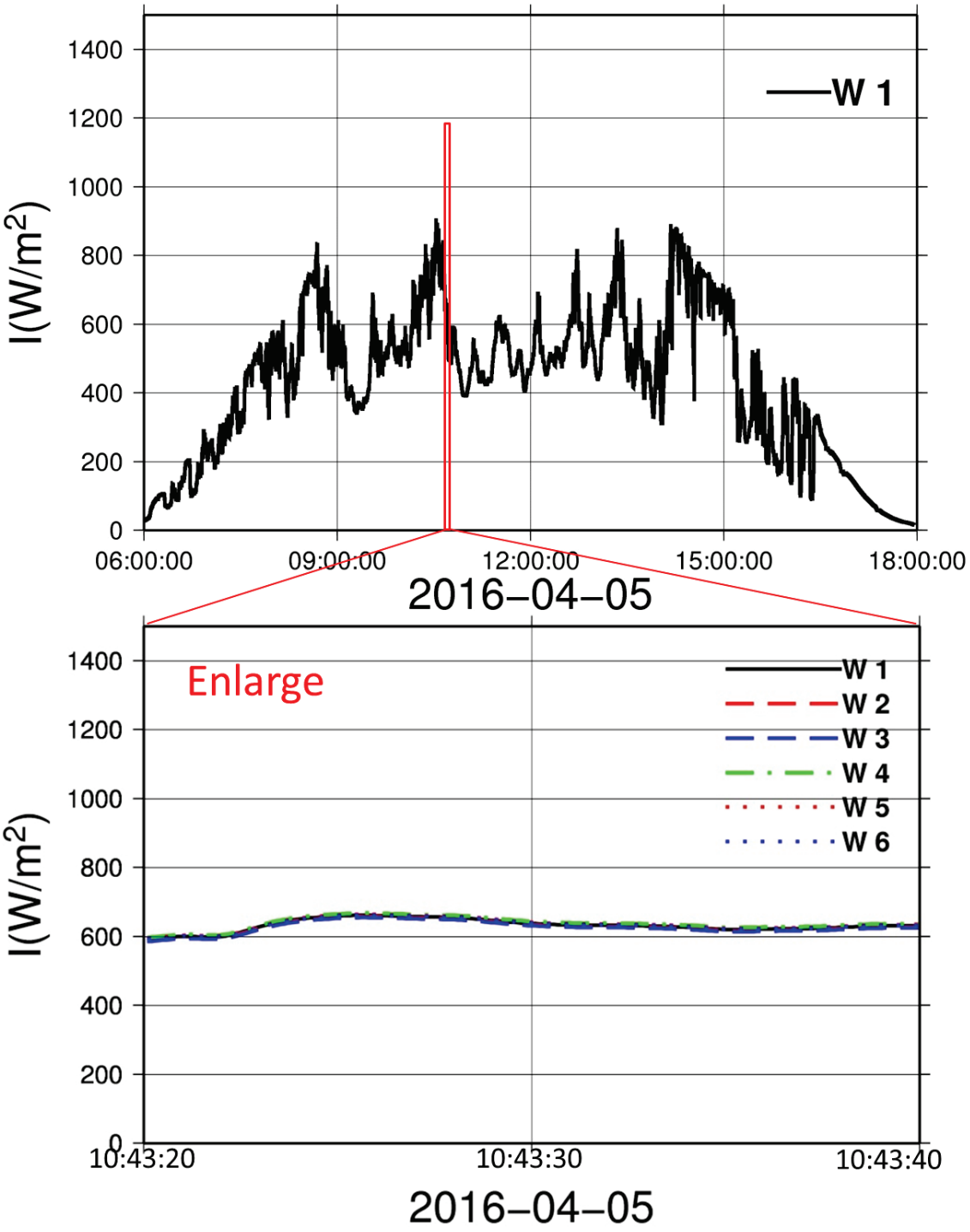

Fig. 4.12 Time series of solar irradiance in a day and in short period (20 s) in a cloudy day with stratus clouds.

4.4 Summary

In this study, solar irradiance is observed using several high-speed pyranometers named PV module sensors (PVMSs), and their temporal instability and spatial nonuniformity are analyzed. The speed and direction of cloud shadows moving on them, and hence the speed and direction of the cloud itself, are evaluated from the time delay on the irradiance time series observed with several PVMSs. Next, on the basis of cloud distributions, weather conditions are classified into four types, and the characteristics of solar irradiance fluctuations caused by clouds are examined. Marked temporal fluctuations and spatial variations are observed under weather conditions with cumulus clouds. The amplitude of irradiance fluctuation reaches 70% of clear-day irradiance at noon in this observation. The spatial nonuniformity evaluated on the basis of the instantaneous difference in irradiance intensity between two PVMSs also reaches 1.8%/m of clear-day irradiance. On the other hand, under weather conditions with layered clouds, the solar irradiance intensity is low, and temporal instability and spatial variation are smaller those weather conditions with cumulus clouds.

Wind speed and cloud movement usually change depending on the height of clouds. The cloud movement is examined in this study but not its height. The difference in the speed of the wind or cloud movement depending on cloud height will be examined in a future study for analyzing solar irradiance fluctuations. Also, the observation error of solar irradiance intensity due to cloud edge effects or others will be analyzed for high-accuracy outdoor PV module performance characterizations.

Reference

1. Tomson, T., and Tamm, G., (2006). Short-term variability of solar radiation. Solar Energy, 80(5), 600-606.
2. Otani, K., Minowa, J., and Kurokawa, K., (1997). Study on areal solar irradiance for analyzing areally-totalized PV systems. Solar Energy Materials and Solar Cells, 47(1-4), 281-288.
3. Barnett, T. P., Ritchie, J., Foat, J., and Stokes, G., (1998). On the space–time scales of the surface solar radiation field. Journal of Climate, 11(1), 88-96.
4. Lave, M., and Kleissl, J., (2010). Solar variability of four sites across the state of Colorado. Renewable Energy, 35(12), 2867-2873.
5. Kariuki, B. W., and Sato, T., (2018). Interannual and spatial variability of solar radiation energy potential in Kenya using Meteosat satellite. Renewable Energy, 116, 88-96.
6. Perez, R., Kivalov, S., Schlemmer, J., Hemker, K., and Hoff, T. E., (2012). Short-term irradiance variability: Preliminary estimation of station pair correlation as a function of distance. Solar Energy, 86(8), 2170-2176.
7. Hoff, T. E., and Perez, R., (2012). Modeling PV fleet output variability. Solar Energy, 86(8), 2177-2189.
8. Tripathy, S. K., Mitra, I., Heinemann, D., Giridhar, G., and Gomathinayagam, S., (2017). Impact assessment of short-term variability of solar radiation in Rajasthan using SRRA data. Renewable and Sustainable Energy Reviews, 78, 798-806.
9. Duchon, C. E., and O'Malley, M. S., (1999). Estimating cloud type from pyranometer observations. Journal of Applied Meteorology, 38(1), 132-141.
10. Sandra, K., (2011). Cumulus and stratus Clouds Microstructure. Number 5, Volume

VI.

Chapter 5 Solar irradiance enhancement due to cloud edge effects

5.1 Introduction

Clouds significantly weaken global solar irradiance on the ground. However, enhancement of solar irradiance rarely happens under specific cloud conditions, and the solar irradiance intensity is higher in a cloudy day than that in a clear sky, and sometimes even it is higher than that at the top of the atmosphere (Wyser et al., 2002; Cede et al., 2002; Gu et al., 2001; Pfister et al., 2003; Schade et al., 2007; Hansen et al., 2010; Berg et al., 2011; Piacentini et al., 2011; Yordanov et al., 2012; Luoma et al., 2012; Lappalainen et al., 2015; Vamvakas et al., 2017; Tapakis et al., 2014; Almeida et al., 2014; Andrade et al., 2016; Inman et al., 2016; Piedehierro et al., 2014; Thuillier et al., 2013; Tomson et al.,2013; Tomson et al., 2014; Tzoumanikas et al., 2016) . This phenomenon has not been examined well in meteorology, because its duration is too short to measure for ordinary meteorological observation instruments, and its impact on energy circulation in the atmosphere is negligible. For photovoltaic (PV) systems, excessive power output from PV modules under an enhanced irradiance poses a risk of damage to inverters (Luoma et al., 2012; Burger et al., 2006; Chen et al., 2010; Chen et al., 2013). The solar constant is 1,366 W/m2, and solar irradiance observed on the ground does not exceed this value without its enhancement. The largest observed global solar irradiance reported in the literature is 1,891 W/m2, which was observed by Gueymard (2017) at the foothills of the Rocky Mountains in Colorado using several kinds of radiometers at 1 s interval. The irradiance is enhanced by 190% compared with that under a clear sky. Emck and Richter (2008) reported a value of 1,832 W/m2 as the global irradiance observed at a place

1,900 m in altitude in the Southern Ecuadorian Andes Mountains near the equator, and it has been the second largest record of measured global solar irradiance reported to date. The duration of enhanced solar irradiance is very short, in the range from 20 to 140 s (Pfister et al., 2003; Schade et al., 2007) and hence fast observation instruments are necessary for detection of transient phenomena.

While this phenomeon, solar irradiance enhancement is observed, its physical mechanics have also been investigated and several tentative theories have been proposed. Segal and Davis (1992) assumed that sunlight is reflected at the edges of cumulus cloud and converges at a certain point on the ground. Piacentini et al. (2011) also explained that direct solar irradiance is reflected at cloud edges and global irradiance is enhanced when cumulus clouds exist around the sun and the cloud coverage rate is from 50 to 90%. On the other hand, Yordanov and coworkers (Yordanov et al., 2012; Yordanov et al., 2015) and Pecenak et al. (2016) suggested not the reflections, but strong forward Mie scattering within clouds around the solar disk as a cause of the enhancement. Gueymard (2017) indicated that a high-albedo ground condition induces a high diffusion rate of irradiance on the ground and therefore it may be a cause of solar irradiance enhancement. Although several assumptions regarding the cause of solar irradiance enhancement have been proposed, the physical mechanism underlying the enhancement has not been clarified.

In this study, solar irradiance enhancement is detected by observation with high-speed pyranometers, and its characteristics and mechanism are discussed. Their statistical properties are also analyzed

5.2 Irradiance enhancement and weather conditions

Some events of solar irradiance enhancement were detected. One example is selected here for the following discussion. Two time series of solar irradiances observed with a

PVMS are shown in Fig. 5.1. One is an enhanced solar irradiance observed on a cloudy day, June 23, 2016, and the other on a clear day, June 10, 2016, which is the clear day nearest the cloudy day. The solar irradiance on a cloudy day fluctuates markedly around noon and sometimes exceeds that under a clear sky and the solar constant of 1,366 W/m2, as indicated in Fig. 5.1(b). The solar irradiance intensity reaches 1,629 W/m2 and it increases by 155% compared with that on a clear day and by 119% compared with the solar constant. Figure 5.2 shows the cloud distribution images taken by the sky camera in the early morning, near noon time, and in the afternoon, and their irradiances are weak, enhanced, and fine, respectively, as shown in Fig. 5.1. In this figure, at 08:30:00, the entire sky is covered by thick layered clouds and the sun cannot be found in the image. As in Fig. 5.1, the enhancement occurred around 11:08:00. At that time, the sky was covered with cumulus clouds with gaps, and the clouds near the sun, which was behind the shadow blade, appear extremely bright owing to the irradiance diffused by cloud water particles. The solar irradiance is enhanced by the superimposition of the scattered irradiance on the direct irradiance passing through a gap in cloud.

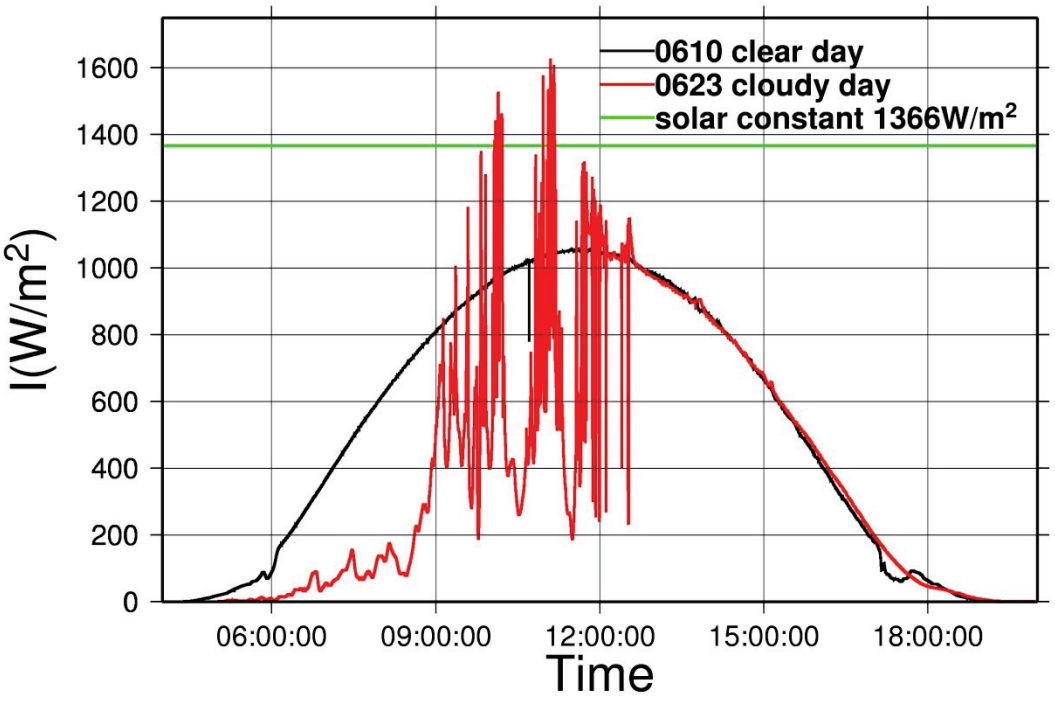

(a)

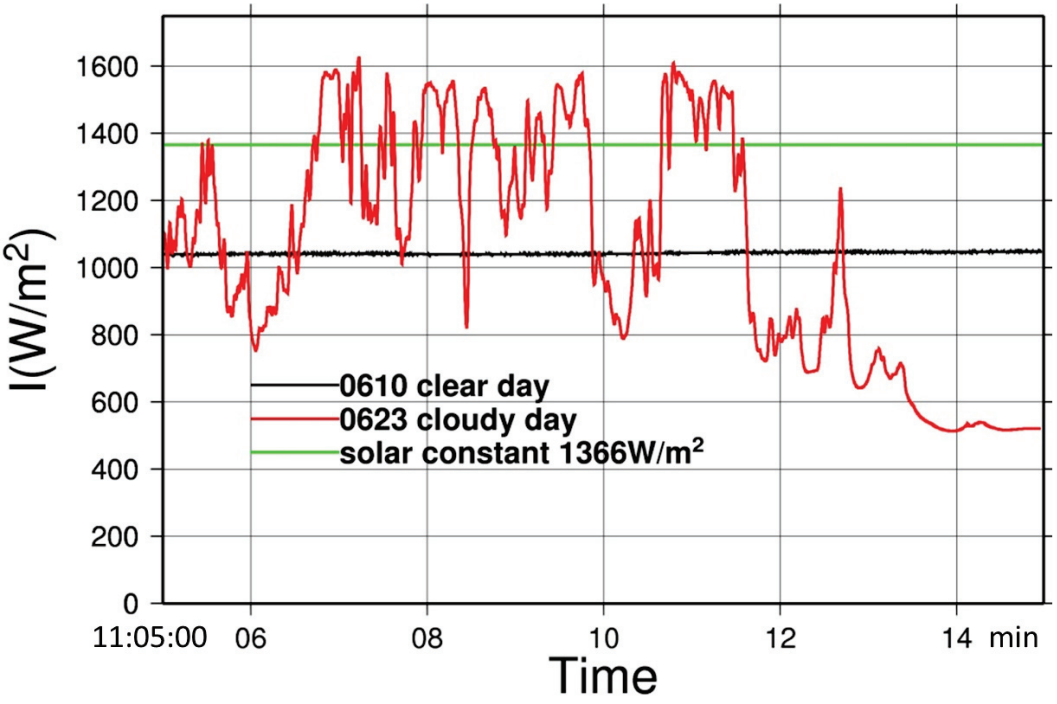

(b)

Fig. 5.1 Time series of solar irradiances. (June 23, 2016 contains enhanced irradiance. 2016/06/10 is the nearest clear day) (b) Solar irradiance in the period with the largest enhancement

Fig. 5.2 Cloud images taken by sky camera, the black bands in them are shadow blades.

(June 23, 2016. 8:30:00, 11:05:00 and13:00:00)

Table 5.1 shows the number of days when solar irradiance enhancement occurred, that is, irradiance with the intensity more than 100 W/m^2 higher than that of reference clear-sky day, in each month from March 2016 to December 2017. The irradiance of the reference clear-sky day is evaluated with the interpolation of the ones on the nearest clear days before and after the target day. In the table, the enhancement seems to be observed more frequently in summer (from June to August) than other seasons. Cumulus clouds can be found in this season in Japan, because the temperature difference between the upper and lower layers in the atmosphere is large. From this result, it is considered that cumulus clouds cause the enhancement of solar irradiance.

Table 5.1 Number of days when solar irradiance enhancement occurred. (Irradiance is defined to be enhanced when its intensity is more than100 W/m2 higher than that on a clear day from Mar. 2016 to Dec. 2017.)

Number of days in a month

Month / Year	1	2	3	4	5	6	7	8	9	10	11	12
2016			3	9	7	13	12	16	18	9	12	10
2017	9	18	13	12	12	9	10	20	12	9	4	8
Average	11.14											

As explained in the previous section, Yordanov and coworkers (Yordanov et al., 2012; Yordanov et al., 2015) and Pecenak et al. (2016) suggested that forward Mie scattering within clouds is a cause of the enhancement. The cloud distribution images in Fig. 5.2 support their suggestion. The mechanism of solar irradiance enhancement observed in this study is that the strong diffuse irradiance scattered at the edges of cumulus clouds near the sun is superimposed on the direct irradiance passing through a gap in the clouds, as illustrated in Fig. 5.3. The solar irradiance at the observation site is enhanced by the superimposition of the strong diffuse irradiance on the direct irradiance. In the other cases when the enhancement was detected, similar clouds and scattered irradiance characteristics as in Fig. 5.2 were found in the pictures taken by the sky camera. As an optical process of the enhancement at the edges of cloud's edges in Piacentini et al. (2011) suggested the reflection of the direct solar irradiance; however, clouds consist of numerous small cloud-water particles, which cannot constructs planes for the reflections at the clouds surface. From this discussion, the forward Mie scattering is more accurate as the optical process at cloud's edges in the enhancements.

As shown in Figs. 5.1 and 5.2, the clouds have disappeared in the afternoon and the irradiance becomes stable under a clear sky. Several time series of the enhanced irradiance are found in the observation period, and in most of these series, the enhancements are observed in the transient phase when the weather changes from very cloudy to clear.

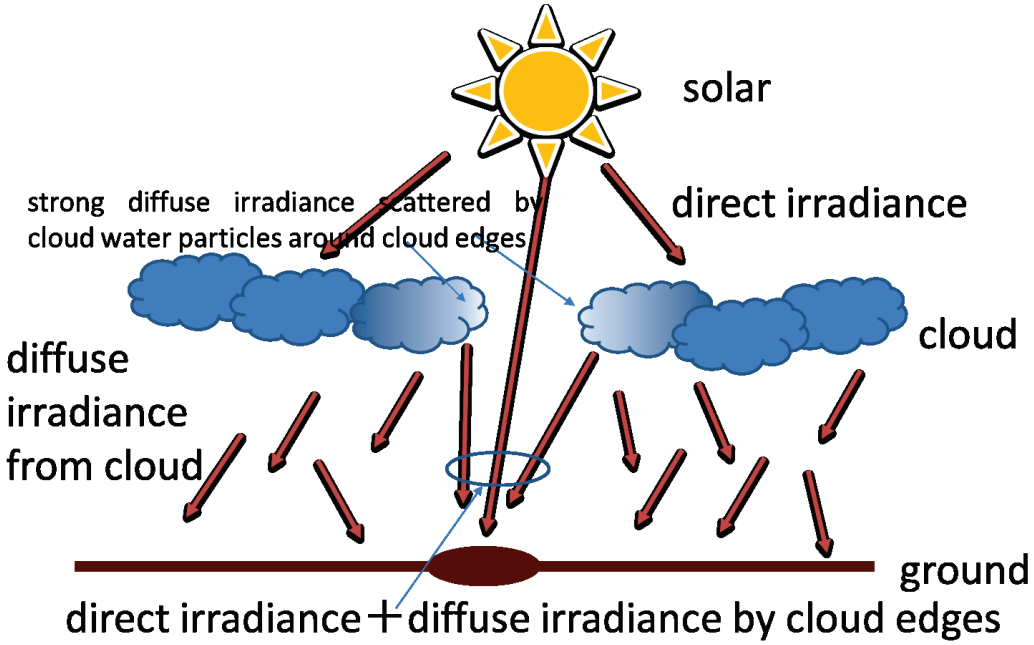

Fig. 5.3 Image of solar irradiance enhancement mechanism due to cloud edges

The enhancements of the irradiance are also observed in the morning or afternoon. Figure 5.4 shows solar irradiance time series on June 10 and 17, 2016. The irradiance intensity on June 17 fluctuated the whole day and sometimes exceeded that on a clear-day on June 10 as shown in Fig. 5.4(a). Figure 5.4(b) shows enhanced irradiance observed at around 9:05:00, and the cloud pattern observed with the sky camera at the corresponding time is shown in Fig. 5.5. The same as in the previous case, the enhancement occurred in the presence of cumulous clouds with gaps as shown in Figs. 5.4 and 5.5.

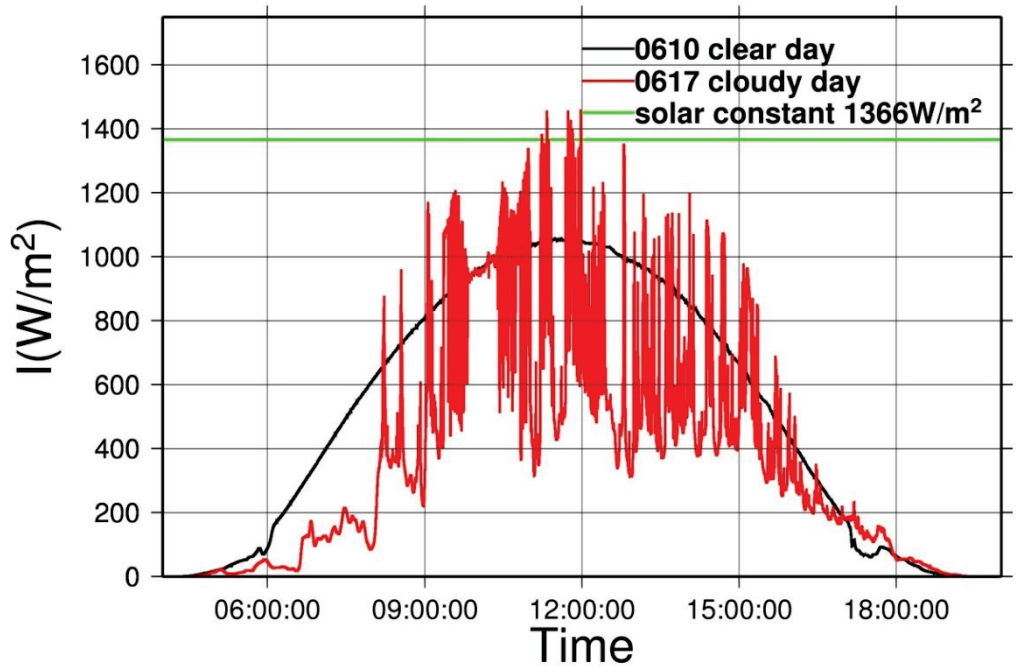

(a)

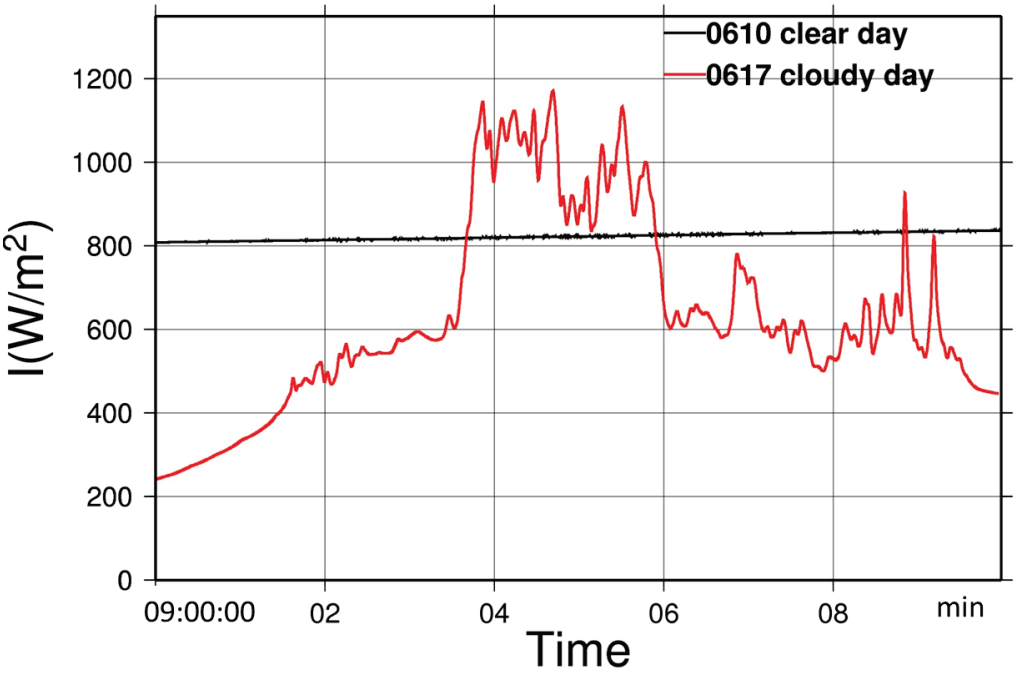

(b)

Fig. 5.4 Time series of solar irradiance. (June 17, 2016 contains enhanced irradiance. June 10, 2016 is the nearest clear day.) (a)Solar irradiance in a day(b)Short fluctuation of solar irradiance around time 09:00:00

Fig. 5.5 Cloud image taken by sky camera.

The black band is the shadow blade. (09:05:00, June 17, 2016.)

The relationship between the solar irradiance enhancement and the weather conditions is discussed further using weather maps. Figure 5.6 shows the ground weather maps on June 23, 2016, which is the same day as for the data shown in Figs. 5.1 and 5.2. The observation site is indicated by a green dot on the map. On that day, meteorological fronts passed near the site. The fronts around Japan are generated as interfaces between a southern warm and wet air mass and a northern cold and dry mass, and clouds including cumulus and cumulonimbus clouds are generated along the fronts. Not only on that day, but also most of the other days when the enhancement was observed, meteorological fronts passed near the observation site as seen on meteorological maps. It means that cumulus or cumulonimbus clouds generated along meteorological fronts cause the enhancement of solar irradiance.

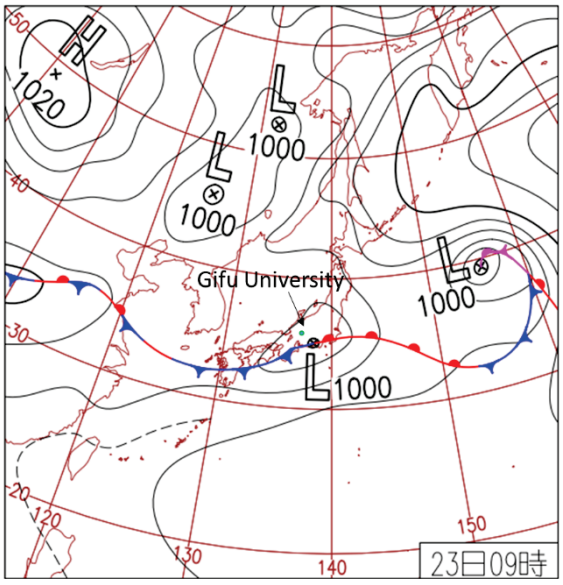

Fig. 5.6 Weather map (June 23, 2016. Categories added and created according to Japan Meteorological Agency.)

5.3 Statistical properties of solar irradiance enhancements

Solar irradiance enhancement was detected frequently at the observation site. Figure 5.7 shows the time series of enhanced solar irradiance in April, 2016. In the figure, the irradiance intensities on a clear day, April 15, are plotted with a black line as the reference. The irradiance enhancement occurred on almost one-third of days in this month. It was also observed in other months, particularly in summer. As explained in the previous section, the number of days the solar irradiance enhancement occurred in each month is shown in Table 5.1. The irradiance enhancement is observed in 245 days in this target period. From this result, the average occurrence frequency is 11.14 days in a month, which is almost one-third of days in a month.

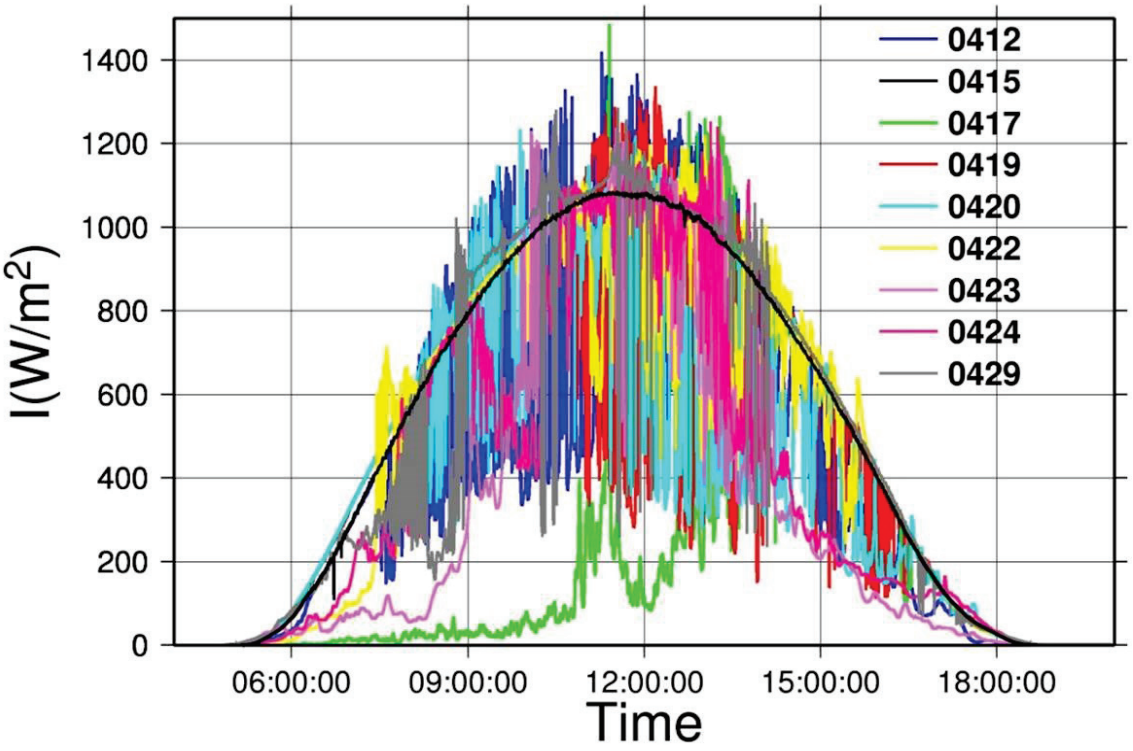

Fig. 5.7 Time series of solar irradiance of days when the irradiances are enhanced

The irradiance enhancement events are detected from observation data and their statistical properties are analyzed. The enhancement events are defined those in which the solar irradiance intensity exceeds that on a clear day. The irradiance intensity on a clear day is evaluated with the interpolation of those on the nearest clear days before and after the target day. Three parameters, i.e., amplification, duration, and volume, are defined here for an enhanced event as illustrated in Fig. 5.8, and they are calculated from the maximum intensity, the elapse time, and the area of time series, respectively. Enhancement events are selected from time series irradiance when the amplification exceeds unity. The target period is from March 6, 2016 to July 31, 2016 from 9:00:00 to 15:00:00 every day. The ten events largest in amplification are listed in Table 5.2. 63,511 enhancement events were detected in the period, and the amplification and duration of the largest event are 1.629 and 45.7 s, respectively. The amplification of the top-ten events

exceeds 1.5, and the longest duration listed in the table is more than 4 min.

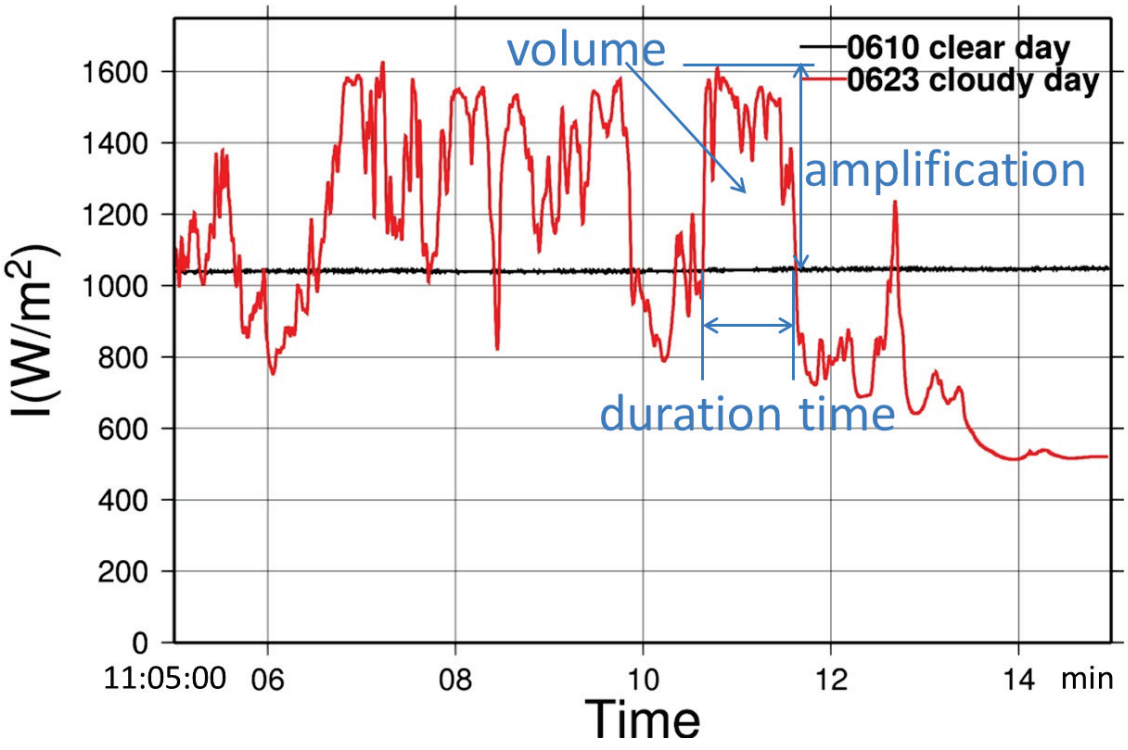

Fig. 5.8 Enlarged time series of enhanced solar irradiance and definition of parameters for enhanced events (June 23, 2016, 11:05:00-11:15:00)

Table 5.2 Ten largest enhanced irradiances

Rank order	Amplification	Duration time [s]	Volume[s]
1	1.629	45.7	14.00
2	1.619	284.8	94.51
3	1.606	94.4	31.82
4	1.585	54.0	14.51
5	1.583	102.8	37.14
6	1.572	113.4	37.33
7	1.569	52.2	13.91
8	1.565	80.8	22.74
9	1.552	60.3	24.91
10	1.551	164.5	59.68

Figure 5.9 shows the occurrence frequencies of amplification, duration, and volume of the enhancement events. From Fig. 5.9(a), the amplifications of most of the events are less than 1.2, but the events with large amplitudes exceeding 1.5 are also found. Also from Figs. 5.9(b) and 5.9(c), the events with a short duration (less than 5 s) or a small volume (less than 3 s) are dominant, but some events have long durations or large volumes exceeding 20 s.

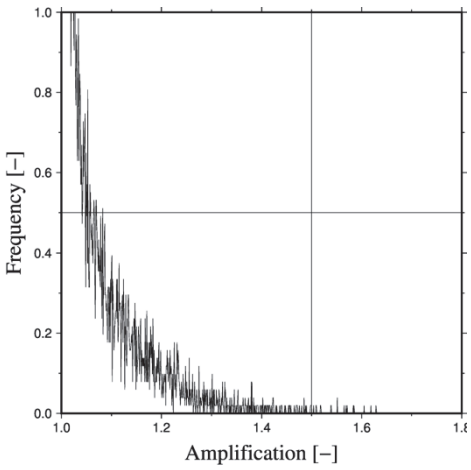

(a) Occurrence frequency of amplification

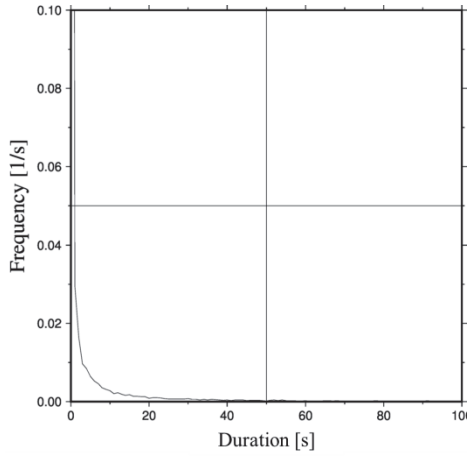

(b) Occurrence frequency of duration

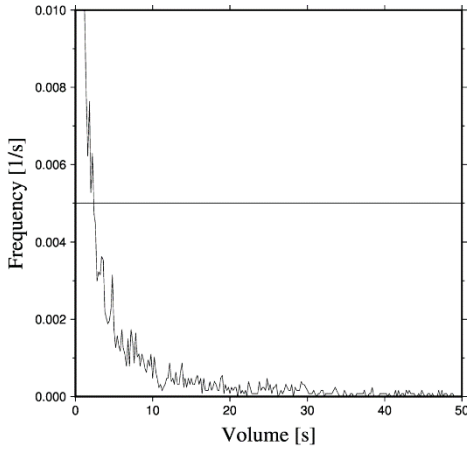

(c) Occurrence frequency of volume

Fig. 5.9 Occurrence frequencies of parameters, i.e. amplification, duration, and volume of enhanced irradiances

The correlations of amplification with duration and volume are shown in Figs. 5.10(a) and 5.10(b), respectively. Many data points are plotted along the axes in Fig. 5.10(a), which means that there are events with either large amplifications or long durations. However, the events with both large amplifications which exceeding 1.3 and long durations of more than 500 s are not found in the figure. On the other hand, it is found in Fig. 5.10(b) that some events have both large amplitudes and large volumes exceeding 100 s. The correlation between the amplification and volume of solar irradiance enhancement is not clear.

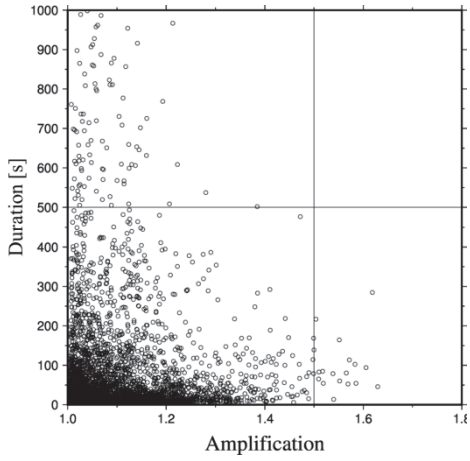

(a)

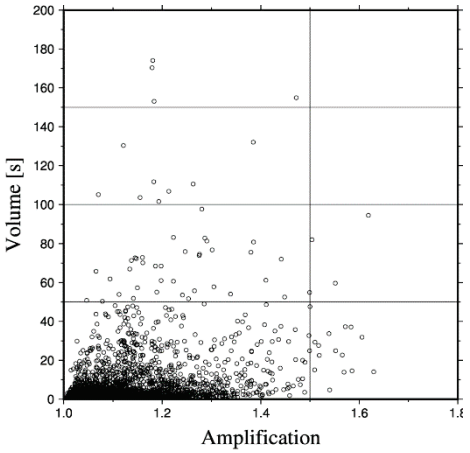

(b)

Fig. 5.10 Correlations between amplification and duration time (a), or volume (b)

Solar irradiance enhancement is also detected from the irradiance data obtained with the ordinary short-wave pyranometers32) used for the calibration of the PVMSs here. Its sampling rate is 1 min; therefore, the enhancement events whose duration is twofold longer than the sampling rate, i.e., 2 min, can be detected. The irradiance time series observed on a cloudy day, June 23, 2016, and on the nearest clear day, June 10, observed using the pyranometers are plotted in Fig. 5.11. The target date and time are the same as those in Fig. 5.1 with the PVMS. On the short-period time series, Fig. 5.11(b), the irradiance observed with a PVMS is also plotted. As shown in this figure, the enhancement events are detected with the ordinary pyranometers. However, detailed profiles of the events cannot be presented, or events with short durations cannot be detected, as indicated from the comparison with irradiance observed with the PVMS in Fig. 5.11(b). The fluctuations of enhancement events are marked and their time scale is short; therefore, high-speed pyranometers, such as PVMSs are required for the observation of solar irradiance enhancement.

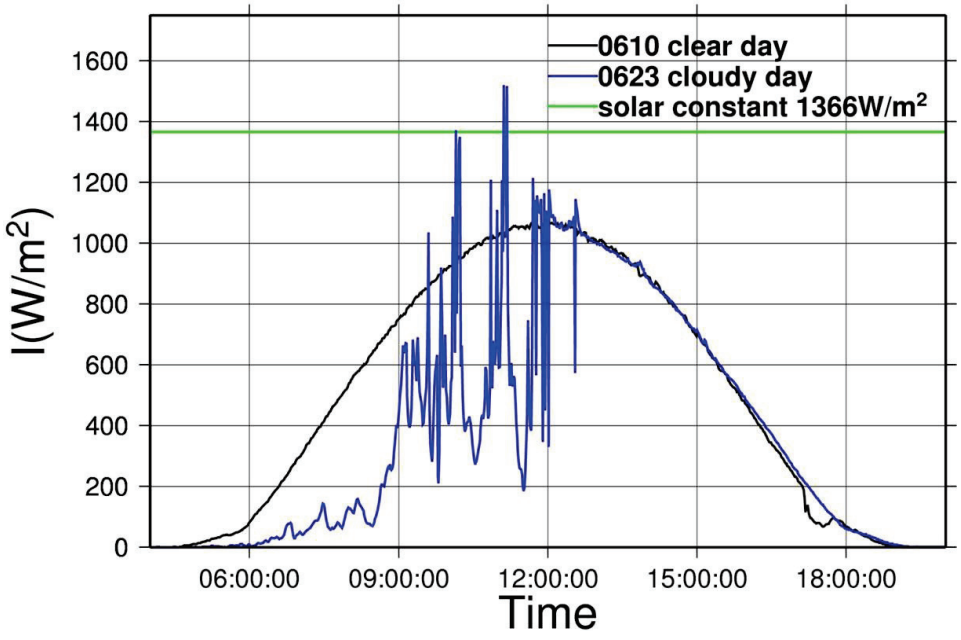

(a)

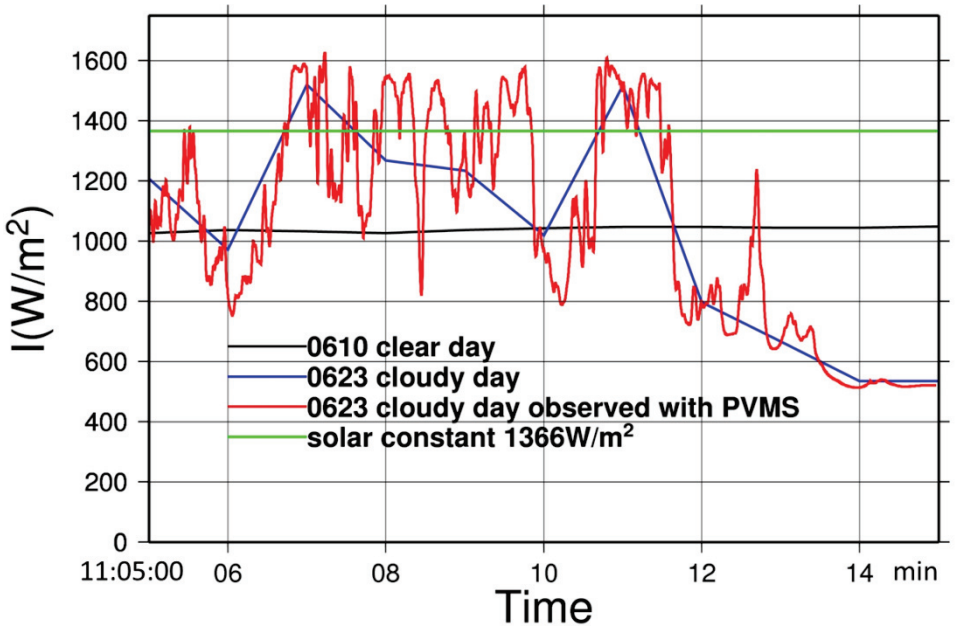

(b)

Fig. 5.11 Time series of solar irradiance observed with ordinary pyranometers. (June 23, 2016 contains enhanced irradiance. June 10, 2016 is the nearest clear day). (a).Solar irradiance on a day,(b).Short fluctuation of solar irradiance around time 11:10:00. Irradiance observed with a PVMS is also plotted

5.4 Summary

In this chapter, enhancement of solar irradiance observed using high-speed pyranometers and a sky camera was analyzed. The irradiance enhancement occurs frequently and was detected in almost one-third of the days in a month. From the observation with the sky camera, the enhancement occurred owing to the superimposition of the diffuse irradiance scattered at the edges of cumulus clouds near the sun on the direct irradiance passing through a gap in the clouds. It is also found that the enhancement is induced when the cumulus or cumulonimbus clouds generated along meteorological fronts pass near the site. Events with enhanced solar irradiance were detected for five months and their amplifications, durations, and volumes were analyzed statistically. The amplifications of some of the largest enhancement events exceeded 1.6, and their durations were several tens of seconds or several minutes. Statistical analyses showed events with either large amplifications or long durations, but not events with both large amplifications and long durations were found.

Reference

1. Wyser, K., O'Hirok, W., Gautier, C., and Jones, C., (2002). Remote sensing of surface solar irradiance with corrections for 3-D cloud effects. Remote Sensing of Environment, 80(2), 272-284.
2. Cede, A., Blumthaler, M., Luccini, E., Piacentini, R. D., and Nuñez, L., (2002). Effects of clouds on erythemal and total irradiance as derived from data of the Argentine Network. Geophysical Research Letters, 29(24).
3. Gu, L., Fuentes, J. D., Garstang, M., da Silva, J. T., Heitz, R., Sigler, J., and Shugart, H. H., (2001). Cloud modulation of surface solar irradiance at a pasture site in southern Brazil. Agricultural and Forest Meteorology, 106(2), 117-129.
4. Pfister, G., McKenzie, R. L., Liley, J. B., Thomas, A., Forgan, B. W., and Long, C. N., (2003). Cloud coverage based on all-sky imaging and its impact on surface solar irradiance. Journal of Applied Meteorology, 42(10), 1421-1434.
5. Schade, N. H., Macke, A., Sandmann, H., and Stick, C., (2007). Enhanced solar global irradiance during cloudy sky conditions. Meteorologische Zeitschrift, 16(3), 295-303.
6. Hansen, C. W., Stein, J. S., and Ellis, A., (2010). Statistical criteria for characterizing irradiance time series. Sandia Report, SAND2010-7314.
7. Berg, L. K., Kassianov, E. I., Long, C. N., and Mills, D. L., (2011). Surface summertime radiative forcing by shallow cumuli at the Atmospheric Radiation Measurement Southern Great Plains site. Journal of Geophysical Research: Atmospheres, 116(D1).
8. Piacentini, R. D., Salum, G. M., Fraidenraich, N., and Tiba, C., (2011). Extreme total solar irradiance due to cloud enhancement at sea level of the NE Atlantic coast

of Brazil. Renewable Energy, 36(1), 409-412.

9. Yordanov, G. H., Midtgard, O. M., Saetre, T. O., Nielsen, H. K., and Norum, L. E., (2012). Overirradiance (cloud enhancement) events at high latitudes. In Photovoltaic Specialists Conference (PVSC), Volume 2, IEEE 38th (pp. 1-7). IEEE.
10. Luoma, J., Kleissl, J., and Murray, K., (2012). Optimal inverter sizing considering cloud enhancement. Solar energy, 86(1), 421-429.
11. Lappalainen, K., and Valkealahti, S., (2015). Recognition and modelling of irradiance transitions caused by moving clouds. Solar Energy, 112, 55-67.
12. Vamvakas, I., and Kazantzidis, A., (2017). On the Enhancement of Solar Irradiance Due to the Presence of Clouds at Patras, Greece. In Perspectives on Atmospheric Sciences (pp. 1169-1174). Springer International Publishing.
13. Tapakis, R., and Charalambides, A. G., (2014). Enhanced values of global irradiance due to the presence of clouds in Eastern Mediterranean. Renewable Energy, 62, 459-467.
14. Almeida, M. P., Zilles, R., and Lorenzo, E., (2014). Extreme overirradiance events in São Paulo, Brazil. Solar Energy, 110, 168-173.
15. Andrade, R. C. de., and Tiba, C., (2016). Extreme global solar irradiance due to cloud enhancement in northeastern Brazil. Renewable Energy, 86, 1433-1441.
16. Inman, R. H., Chu, Y., and Coimbra, C. F., (2016). Cloud enhancement of global horizontal irradiance in California and Hawaii. Solar Energy, 130, 128-138.
17. Piedehierro, A. A., Antón, M., Cazorla, A., Alados-Arboledas, L., and Olmo, F. J., (2014). Evaluation of enhancement events of total solar irradiance during cloudy conditions at Granada (Southeastern Spain). Atmospheric research, 135, 1-7.
18. Thuillier, G., Perrin, J. M., Keckhut, P., and Huppert, F., (2013). Local enhanced

solar irradiance on the ground generated by cirrus: measurements and interpretation. Journal of applied remote sensing, 7(1), 073543-073543.

19. Tomson, T., (2013). Transient processes of solar radiation. Theoretical and applied climatology, 112(3-4), 403-408.
20. Tomson, T., (2014). Dynamic behaviour of diffuse solar radiation. Theoretical and applied climatology, 117(3-4), 399-402.
21. Tzoumanikas, P., Nikitidou, E., Bais, A. F., and Kazantzidis, A., (2016). The effect of clouds on surface solar irradiance, based on data from an all-sky imaging system. Renewable Energy, 95, 314-322.
22. Burger, B., and Rüther, R., (2006). Inverter sizing of grid-connected photovoltaic systems in the light of local solar resource distribution characteristics and temperature. Solar Energy, 80(1), 32-45.
23. Chen, S., Li, P., Brady, D., and Lehman, B., (2010). The impact of irradiance time behaviors on inverter sizing and design. In Control and Modeling for Power Electronics (COMPEL), IEEE 12th Workshop on (pp. 1-5).
24. Chen, S., Li, P., Brady, D., and Lehman, B., (2013). Determining the optimum grid-connected photovoltaic inverter size. Solar Energy, 87, 96-116.
25. Gueymard, C. A., (2017). Cloud and albedo enhancement impacts on solar irradiance using high-frequency measurements from thermopile and photodiode radiometers. Part 2: Performance of separation and transposition models for global tilted irradiance. Solar Energy.
26. Emck, P., and Richter, M., (2008). An upper threshold of enhanced global shortwave irradiance in the troposphere derived from field measurements in tropical mountains. Journal of Applied Meteorology and climatology, 47(11), 2828-2845.

27. Segal, M., and Davis, J., (1992). The impact of deep cumulus reflection on the ground-level global irradiance. Journal of Applied Meteorology, 31(2), 217-222.
28. Yordanov, G. H., Saetre, T. O., and Midtgård, O. M., (2015). Extreme overirradiance events in Norway: 1.6 suns measured close to 60° N. Solar Energy, 115, 68-73.
29. Pecenak, Z. K., Mejia, F. A., Kurtz, B., Evan, A., and Kleissl, J., (2016). Simulating irradiance enhancement dependence on cloud optical depth and solar zenith angle. Solar Energy, 136, 675-681.
30. http://www.data.jma.go.jp/fcd/yoho/data/hibiten/2016/201606.pdf.

Chapter 6 Filtering method of detecting solar irradiance conditions for PV module performance characterization under unstable irradiance

6.1 Introduction

Fluctuations of solar irradiance usually exist with variations in time and space. The former is defined as temporal instability, and the latter is defined as spatial nonuniformity. The temporal fluctuations of solar irradiance have already been investigated, and numerous studies have been reported about them in both short (e.g., in d, h, min or s) (Gansler et al., 1995; Otani et al., 1997; Jurado et al., 1995; Tomson et al., 2006; Stein et al., 2012; Lave et al., 2015; Lave et al., 2012; Gagné et al., 2016) and long (e.g., years or months) (Willson et al., 1981; Smith et al., 1983; Babu et al., 2001; Kopp et al., 2005; Wilcox et al., 2010; Kopp et al., 2016; Woyte et al., 2001; Woyte et al., 2007) timescales. However, studies about the spatial nonuniformity of solar irradiance are limited, because the space variation in irradiance is relatively difficult to measure compared with time fluctuation. In most reports in which the spatial variation in solar irradiance is discussed, the target distance or area is large (e.g., 4, 10, 30, 100, and 532 km). For the PV module performance characterizations, the spatial variation in solar irradiance on modules should be examined; therefore, the target range in space is about 1 to 10 m. On the other hand, since Hishikawa and coworkers (Hishikawa et al.,2015 ; Fukabori et al., 2015; Hishikawa et al., 2014) employed fast I-V meters for outdoor characterizations, their time scale is in 1 s or less for the characterizations. In this chapter, temporal instability and spatial nonuniformity of solar irradiance, and their relationship are analyzed with field observations using several high-speed pyranometers. Later, a filtering method of

detecting stable irradiance in time and space with a single meter is proposed for highly accurate outdoor PV module performance characterizations.

6.2 Temporal instability and maximum spatial nonuniformity

Two parameters, temporal instability (*TI*) and maximum special nonuniformity *(Max.NU*) are defined here for evaluation of time and space variations from time series data observed with PVMSs. In this study, the six PVMSs are arranged in lines in the west-east and south-north directions to detect the variation in solar irradiance in space. They are evaluated using the following equations;

$$TI = \frac{Irr^1_{max} - Irr^1_{min}}{Irr^1_{max} + Irr^1_{min}} \quad , \tag{6-1}$$

$$Max.NU = max\left[\frac{Irr^L_{max} - Irr^S_{min}}{Irr^L_{max} + Irr^S_{min}}\right]_{ts}^{te} \quad , \tag{6-2}$$

Where $Irr^x{}_{max}$, $Irr^x{}_{min}$ are the maximum and minimum solar irradiance detected using sensor *x* in measurement time. *L* and *S* represent two sensors used to observe high and low solar irradiances, respectively. *te* and *ts* respectively denote the start and end of the measurement time, which corresponds to scanning time of I-V measurement. From these equations, *TI* means the largest difference in solar irradiance in the measurement time detected by a sensor, and $Max.NU$ means the largest difference in irradiance between two sensors. *TI* can be evaluated with a single PVMS; however $Max.NU$ requires two PVMSs for evaluation. This is the reason why the measurement of spatial nonuniformity of the irradiance is relatively difficult compared with that of temporal instability.

Here, the target accuracies in both stability and uniformity are assumed to be both 1 %. As a standard measurement condition, the measurement time with PVMSs is also

assumed to be 200 ms, which is the same as scanning time in a high-speed I-V measurement[1)] for the outdoor PV module performance characterizations. Sensors Nos. 1 and 6 are employed under this condition, and the distance between them is 5.725 m.

April 12, 2016 is selected as the target day of analysis. The time series of solar irradiance observed with PVMSs on that day is indicated in Fig. 6.1. As shown in the figure, irradiance fluctuation was very large on the target day. Such a day with large fluctuations may occur once about every three months. The weather condition on that day photographed with the sky camera is shown in Fig. 6.2. Numerous small cumulus clouds cover the sky as shown in the figure.

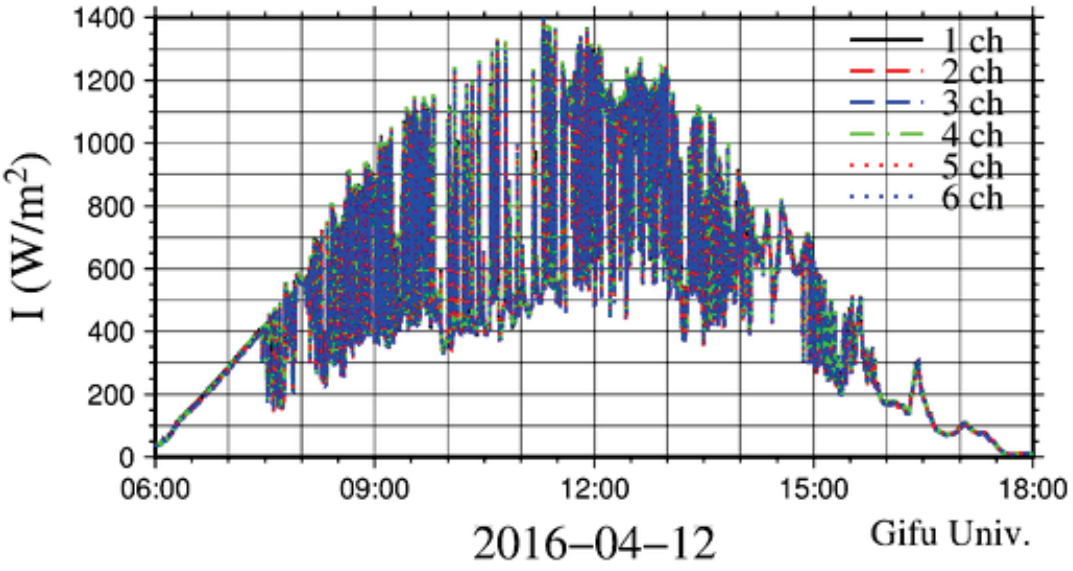

Fig. 6.1 Time series of solar irradiance observed by PVMSs (April 12, 2016).

Fig. 6.2 Clouds' image in the target day taken by sky-camera (April 12, 2016. 12:00:00)

6.3 Temporal instability and maximum spatial nonuniformity of solar irradiance

6.3.1 Effect of distance between PVMSs

To estimate the effects of distance between PVMSs on *TI* and *Max.NU*, the distance between PVMs is changed from the standard measurement condition. The irradiance observed with PVMSs on the target day, April 12, 2016, was analyzed. The correlations between *TI* and *Max.NU* using different PVMS pairs are shown in Fig. 6.3. The PVMSpairs are sensors Nos. 1 and 2, Nos. 1 and 4, and Nos. 1 and 6 along the west-east line, and the distances between pairs are 1.145, 3.435, and 5.725 m, respectively. The measurement time, 200 ms, is the same as that under the standard measurement condition. The yellow area in the figure represents the target range of accuracy, 1%. The horizontal axis is *TI* and the vertical axis is *Max.NU*. It is found that *Max.NU* increases as the distance between PVMSs increases. However, *TI* is constant and independent of the distance between PVMSs in the figure, because it is evaluated with a single PVMS, No. 1.

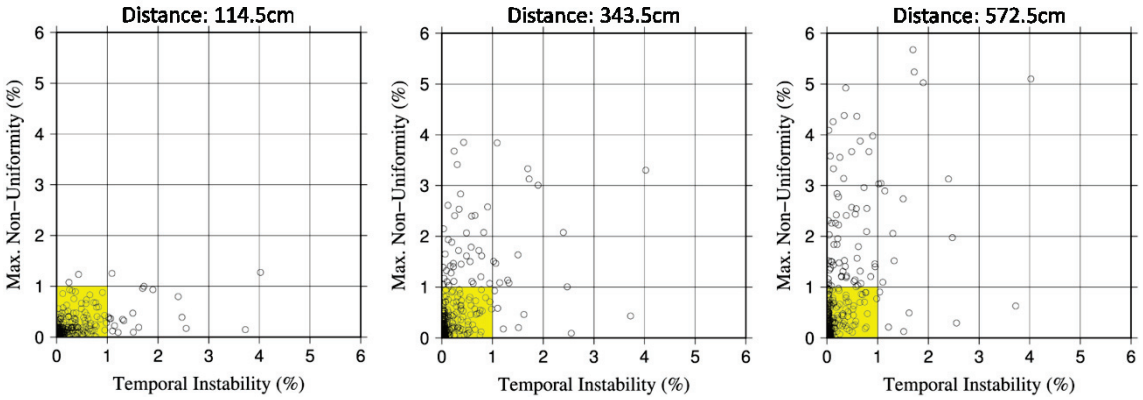

Fig. 6.3 Correlations between *TI* and *Max.NU* with different distance between PVMSs

6.3.2 Effect of Measurement time

The effects of measurement time on *TI* and *Max.NU* are analyzed by changing the time from the standard measurement condition in this section. The distance between PVMSs, 5.725 m, is the same as that under the standard measurement condition. Three cases with different measurement times, 200 ms, 2 s, and 5 s, are analyzed. The correlations between *TI* and *Max.NU* with measurement time are shown in Fig. 6.4. Events with large *Max.NU* increase *TI* with increasing measurement time. On the other hand, *Max.NU* keeps its distribution constant, because the distance between PVMSs is fixed. In the figure, at the measurement time of 5 s, events in which *TI* is less than 1% have a low *Max.NU*, that is, less than 2%. This indicates the possibility of detecting low-*Max.NU* events by referring to *TI* only and employing a longer measurement time.

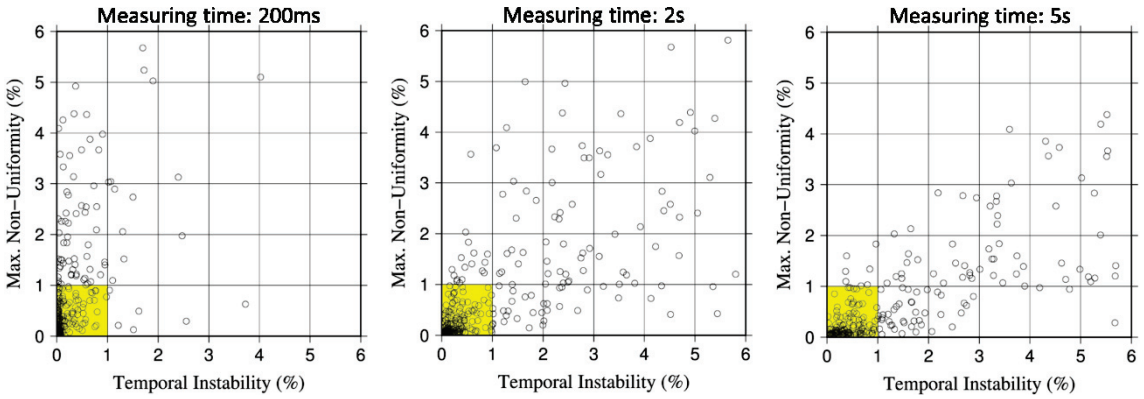

Fig. 6.4 Correlations between *TI* and *Max.NU* with different measurement time

6.3.3 Effect of Repeat counts

Under the standard measurement condition and previous measurements, measurement is performed only once to evaluate *TI* and *Max.NU*. Here, repeated measurements are introduced to evaluate the parameters. The repeated measurement is performed in a time series as shown in Fig. 6.5. Here, the number of repeats is changed from 1 to 5 .The measurement time and distance between PVMSs are the same as those under the standard measurement condition, 200 ms and 5.725 m, respectively. The time interval between measurements is 5 s. Figure 6.6 shows the correlation between *TI* and *Max.NU* when several measurements are performed repeatedly. The parameters *TI* and *Max.NU* are also calculated using Eqs. (6-1) and (6-2); however, the target time for the evaluation is the total measurement time in the repeated measurements. Therefore, the parameters are calculated at once for one repeat measurement. Similarly to the previous case shown in Fig. 6.4, events with large *Max.NU* increase *TI* as the number of repeats increases. In the case when the number of repeats is five, the *Max.NU* of the events in which *TI* is less than 1% is almost less than 1% and the events cluster in the yellow area. This means that when solar irradiance is measured five times, the events with *TI* lower than 1% satisfies the condition of *Max.NU* lower than 1%. This also means that the

events with conditions of both *TI* and *Max. NU* lower than 1% can be selected by applying the 1% threshold only to *TI* observed with a single PVMS. Repeated measurements can be employed as a filtering method of detecting events that satisfy the required conditions of both *TI* and *Max.NU* from observations with a single PVMS.

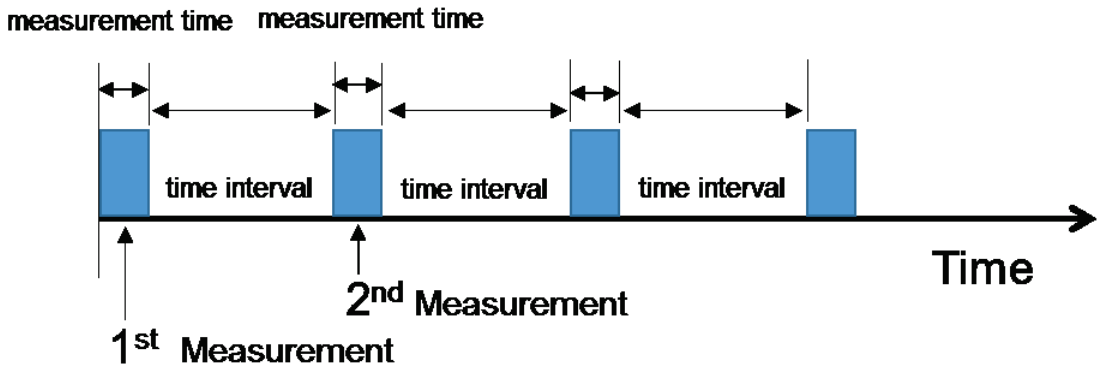

Fig. 6.5 Time series of repeated measurements.

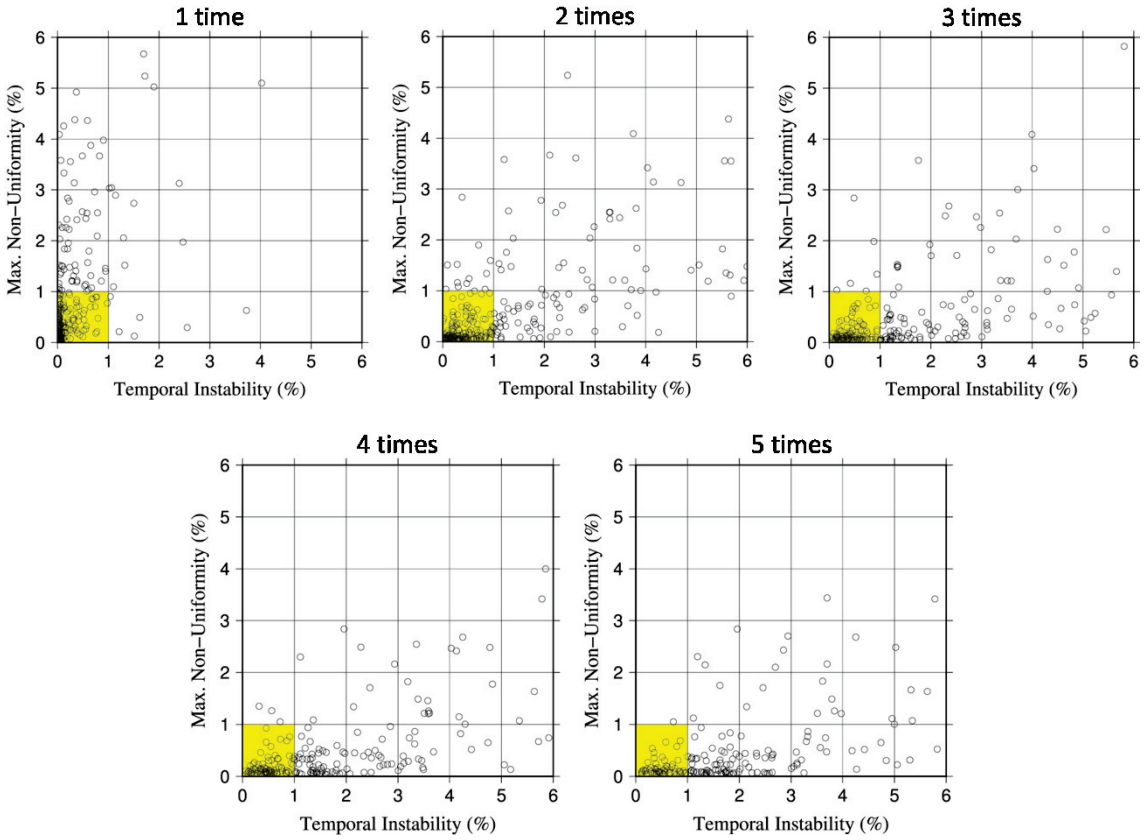

Fig. 6.6 Correlations between *TI* and *Max.NU* with different repeat count

6.3.4 Effect of Time interval

The effects of time interval in the repeated measurements on *TI* and *Max.NU* are discussed here. Figure 6.7 shows the correlation between *TI* and *Max.NU* in the repeated measurements of different time intervals, 5, 10, and 30 s. The PVMS pair distance and measurement time are the same as those under the standard measurement condition, 5.725 m and 200 ms, respectively. The number of repeats is fixed at 5. As shown in this figure, as the time interval increases, *TI* for each event increases, but the effect seems to be smaller than that of measurement time shown in Fig. 6.4. From this result, the time interval in the repeated measurements is less effective for the detection of events with low *TI* and *Max.NU*.

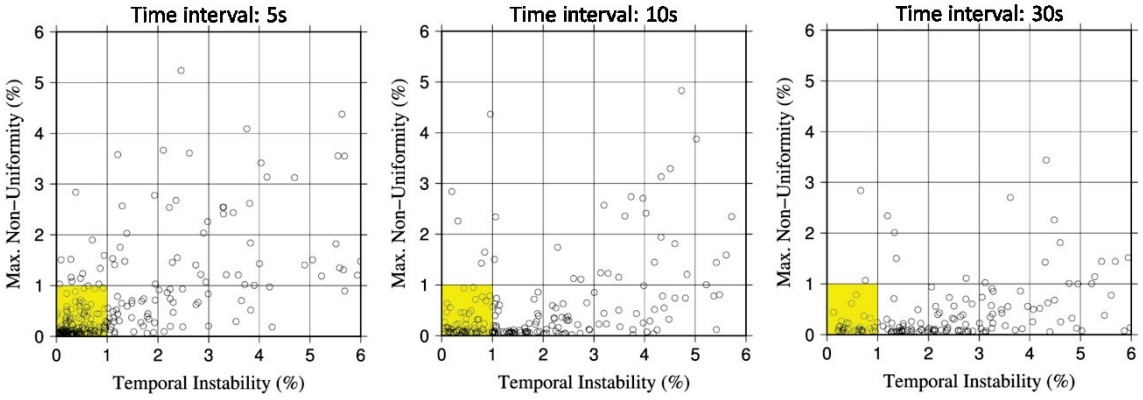

Fig. 6.7 Correlation between *TI* and *Max.NU* with different time interval

6.4 Filter method under various weather conditions

As mentioned in Sect. 6.3.3, the repeated measurements can be employed as a filtering method to select events that satisfy the required condition in both *TI* and *Max.NU* and are appropriate for outdoor PV module performance characterizations. Here, the occupancy rate of events with the required conditions under several weather conditions is discussed. First, weather conditions are categorized into the following four typical cloud distributions from the viewpoint of solar irradiance fluctuations: no clouds (clear sky), a few cumulus clouds, numerous cumulus clouds with gaps, and stratus clouds. Figure 6.8 shows the solar irradiance time series observed with PVMSs and the cloud distributions taken by the sky camera under typical weather conditions. Next, measurement conditions are fixed or selected. The distance between two PVMSs and measurement time are the same as those under the standard measurement condition, 5.725 m and 200 ms, respectively, and the time interval is fixed at 5 s. On the other hand, the number of repeats is changed from 1 to 5. The required conditions for both *TI* and *Max.NU* are the same as above, lower than 1%. The target period in a day is from 9:00:00 to 15:00:00, and the total sample number is 359 in a day.

The number of events and its occupancy rates that satisfy the required conditions under the typical weather conditions are listed in Table 6.1. The rates in the column entitled "*Max.NU*<1% under requirement *TI*<1%" mean the rates of the events in which *TI* and *Max. NU* are less than 1.0%, in the case where *TI* is less than 1%. When this index is high (almost 100%), the stable events that satisfy the conditions for both *TI* and *Max.NU* can be detected by referring to *TI* only from the data observed with a single PVMS.

Under a clear sky, solar irradiance is constant in the measurement time, as shown in

Fig. 6.8(a1), and the occupancy rates of the stable events are 100% in the table. The irradiance under stratus clouds is smaller than those under other conditions, but its fluctuation is smaller than that under cumulus clouds, as shown in Fig. 6.8(a4). The occupancy rates under the stratus clouds are more than 90% in Table 6.1. Under cumulus clouds, as the number of clouds increases, the solar irradiance becomes unstable and its occupancy rate decreases as shown in the figure and table. Under numerous cumulus clouds with gaps, 5 measurements are required to satisfy the conditions, but the occupancy rate of the events in the whole observation period is less than 20%. From Table 6.1, the detection of events with stability in time and uniformity in space becomes more accurate as the number of repeated measurements increases; however, the probability of finding the events decreases with time.

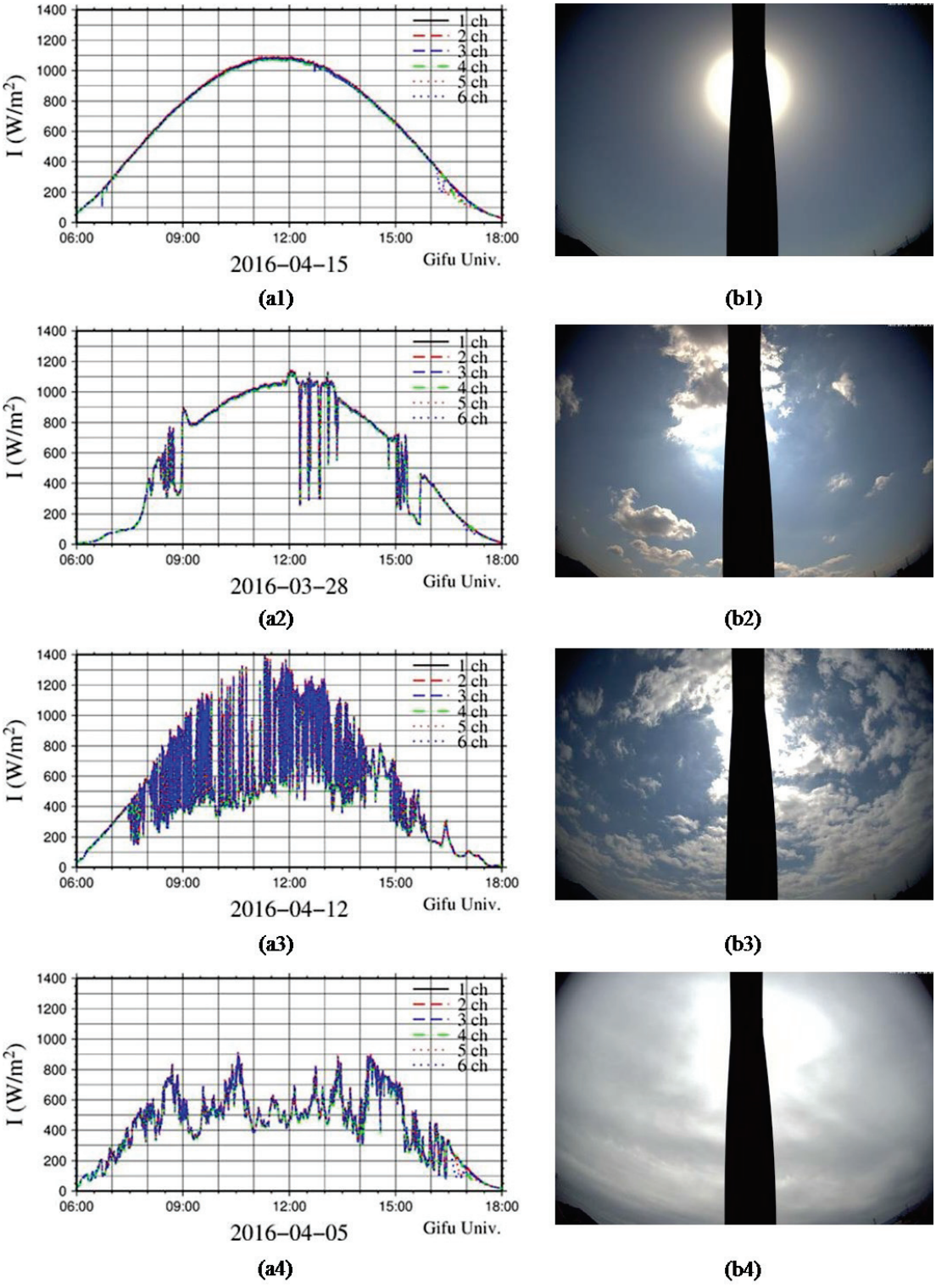

Fig. 6.8 Time series of solar irradiance (a) and corresponding cloud images (b) under four typical cloud conditions (1: no clouds, 2: a few cumulus clouds, 3: numerous cumulus clouds with gaps, 4: stratus clouds).

Table 6.1 Number of events and their occupancy rates that satisfy the conditions *TI* and *Max.NU* under four typical weather conditions.

Weather condition	Repeat count	*TI*<1%	*Max.NU*<1% for requirement *TI*<1%
Clear day	1	359 (100%)	359 (100%)
2016-04-15	2	359 (100%)	359 (100%)
	3	359 (100%)	359 (100%)
	4	359 (100%)	359 (100%)
	5	358 (100%)	358 (100%)
Cloudy day with a few	1	358 (100%)	345 (96%)
cumulus clouds	2	343 (96%)	338 (99%)
2016-03-28	3	336 (94%)	335 (100%)
	4	335 (93%)	334 (100%)
	5	333 (93%)	333 (100%)
Cloudy day with numerous	1	339 (94%)	276 (81%)
cumulus clouds and gaps	2	180 (50%)	168 (93%)
2016-04-12	3	117 (33%)	111 (95%)
	4	89 (25%)	86 (97%)
	5	64 (18%)	63 (98%)
Cloudy day with stratus	1	358 (100%)	345 (96%)
clouds	2	343 (96%)	338 (99%)
2016-04-05	3	336 (94%)	335 (100%)
	4	335 (93%)	334 (100%)
	5	333 (93%)	333 (100%)

6.5 Summary

Characteristics of *TI* and *Max.NU* of solar irradiance and also their relationship are discussed on the basis of field observations in which the timescale is several seconds or less and the area is about the size of the PV module. In the observations, PVMSs and a sky camera are employed to measure solar irradiance and weather conditions, respectively. The use of repeated measurements with a single PVMS is proposed to detect stable irradiance events in time and space for high-accuracy outdoor PV module performance characterizations.

In the repeated measurements of solar irradiance, the characteristics of temporal instability and maximum nonuniformity were examined on the basis of the distance between two PVMSs, measurement time, repeated count, and time interval between measurements. It was found that temporal instability increases with measurement time or repeated count. Also, the maximum nonuniformity increases when the distance between two PVMSs increases. The effect of time interval on temporal instability or nonuniformity is not very obvious. The repeated measurements with a measurement time of 200 ms and a repeat count of 5 are applied to widely strongly fluctuating solar irradiance observed under numerous cumulous clouds and gaps. The events detected under the condition of *TI* less than 1% satisfy the condition of *Max.NU* less than 1%. This means that the events in which irradiance is stable and uniform can be detected only by referring to *TI* obtained by repeated measurements with a single PVMS. This finding indicates that repeated measurements can be employed as a filtering method for monitoring irradiance conditions for high-accuracy outdoor PV module performance characterizations.

Reference

1. Gansler, R. A., Klein, S. A., and Beckman, W. A., (1995). Investigation of minute solar radiation data. Solar energy, 55(1), 21-27.
2. Otani, K., Minowa, J., and Kurokawa, K., (1997). Study on areal solar irradiance for analyzing areally-totalized PV systems. Solar Energy Materials and Solar Cells, 47(1-4), 281-288.
3. Jurado, M., Caridad, J. M., and Ruiz, V., (1995). Statistical distribution of the clearness index with radiation data integrated over five minute intervals. Solar Energy, 55(6), 469-473.
4. Tomson, T., and Tamm, G., (2006). Short-term variability of solar radiation. Solar Energy, 80(5), 600-606.
5. Stein, J. S., Hansen, C. W., and Reno, M. J., (2012, April). The variability index: A new and novel metric for quantifying irradiance and PV output variability. In World Renewable Energy Forum (pp. 13-17).
6. Lave, M., Reno, M. J., and Broderick, R. J., (2015). Characterizing local high-frequency solar variability and its impact to distribution studies. Solar Energy, 118, 327-337.
7. Lave, M., Kleissl, J., and Arias-Castro, E., (2012). High-frequency irradiance fluctuations and geographic smoothing. Solar Energy, 86(8), 2190-2199.
8. Gagné, A., Turcotte, D., Goswamy, N., and Poissant, Y., (2016). High resolution characterisation of solar variability for two sites in Eastern Canada. Solar Energy, 137, 46-54.
9. Willson, R. C., Gulkis, S., Janssen, M., Hudson, H. S., and Chapman, G., (1981). Observations of solar irradiance variability. Science, 211(4483), 700-702.

10. Smith, E. A., Haar, T. H. V., Hickey, J. R., and Maschhoff, B., (1983). The nature of the short period fluctuations in solar irradiance received by the Earth. Climatic Change, 5(3), 211-235.
11. Babu, K. S., and Satyamurty, V. V., (2001). Frequency distribution of daily clearness indices through generalized parameters. Solar Energy, 70(1), 35-43.
12. Kopp, G., Lawrence, G., and Rottman, G., (2005). The total irradiance monitor (TIM): science results. The Solar Radiation and Climate Experiment (SORCE), 129-139.
13. Wilcox, S., and Gueymard, C. A., (2010). Spatial and temporal variability of the solar resource in the United States. Washington, DC: NREL/DoE [National Renewable Energy Laboratory/Department of Energy].
14. Kopp, G., (2016). Magnitudes and timescales of total solar irradiance variability. Journal of Space Weather and Space Climate, 6, A30.
15. Woyte, A., Belmans, R., Nijs, J., (2001). Power flow fluctuations in distribution grids with high PV penetration. In: Proc. 17th EC PV Solar Energy Conference, Munich, Germany, pp. 2414–2417.
16. Woyte, A., Belmans, R., and Nijs, J., (2007). Fluctuations in instantaneous clearness index: Analysis and statistics. Solar Energy, 81(2), 195-206.
17. Hishikawa, Y., Yamagoe, K., Ohshima, H., Tsuno, Y., and Kojima, H., (2015). “New technology for precise outdoor PV module performance measurements,” in Proc. IEEE 42nd Photovolt. Specialist Conf., New Orleans, LA, USA, pp. 1–6.
18. Fukabori, A., Takenouchi, T., Matsuda, Y., Tsuno, Y., and Hishikawa, Y., (2015). “Study of highly precise outdoor characterization technique for

photovoltaic modules in terms of reproducibility," Jpn. J. Appl.Phys., vol. 54, 08KG06.

19. Hishikawa, Y., Fukabori, A., Takenouchi, T., and Tsuno, Y., (2014). "Accurate outdoor measurement technology of PV devices," (in Japanese) in Proc. JSES JWEA Joint Conf., Fukushima, Japan, pp. 289–292.

Chapter 7 Conclusions

The aim of study in this thesis was to investigate the characteristics of solar irradiance fluctuations for photovoltaic module outdoor performance testing. The main goal was to propose an approach to selecting a stable solar irradiance conditions in time and space for high-accuracy photovoltaic module outdoor performance testing.

Cloud is the major factor effecting the solar irradiance fluctuations. In this thesis, we analyzed the relationship between fluctuation of solar irradiance and cloud type and distribution. A quantitative analysis of the magnitude of solar irradiance fluctuations in time and in space were performed in this study. Moreover, the temporal instability and spatial nonuniformity of solar irradiance were analyzed and the connection with the weather conditions or the types and distributions of clouds was discussed. It proposed a filter method for detecting the solar irradiance conditions for PV module outdoor performance characterization even under unstable irradiance was discussed. The relation between instability and nonuniformity of solar irradiance are discussed with observations, and proposed a filtering method to detect stable and uniform solar irradiance condition with required accuracy by observing with only one sensor.

In Chapter 3, the general characteristics of solar irradiance in short period of 1 s in central Japan (Gifu City) are examined. The change rate of solar irradiance in 1 s was used as the index of the characterization of short-period irradiance fluctuations. The occurrence frequency of the solar irradiance change rate in 1 s monthly in one year (from 6 March 2016 to 31 March, 2017) was discussed and calculated here. It is found that in the 95 % of the observation period, the change rate of solar irradiance in 1 s is less than 1.0 % in Japan weather conditions. Compare with the 1 s that the least time interval for precise PV outdoor performance measurement, it is demonstrated that the

stable irradiance condition for the outdoor testing can be found easily under Japanese weather. However, large fluctuations also observed under the characteristics cloud conditions, but the occurrence is low. In the observation, large fluctuation of the irradiance induced when edges of thick clouds pass in front of the sun.

Chapter 4 presents the connection between solar irradiance and cloud type and distribution. First, cloud shadow movement caused by cloud advection is evaluated by considering the distance and the delay of irradiance fluctuations between PVMSs. Simultaneously, the spatial nonuniformity of the irradiance is calculated by instantaneous difference in irradiance intensity between PVMSs. Temporal instability and spatial nonuniformity of solar irradiance under different weather conditions classified on the basis of cloud types and distributions were examined in this chapter. It was found that marked temporal fluctuations and spatial variations are observed under weather conditions with cumulus clouds. The amplitude of irradiance fluctuation reaches 70% of clear-day irradiance at noon in this observation. The spatial nonuniformity evaluated on the basis of the instantaneous difference in irradiance intensity between two PVMSs also reaches 1.8%/m of clear-day irradiance. On the other hand, under weather conditions with layered clouds, the solar irradiance intensity is low, and temporal instability and spatial variation are smaller those weather conditions with cumulus clouds.

In Chapter 5, enhancement of solar irradiance observed using high-speed pyranometers and a sky camera was analyzed. The irradiance enhancement occurs frequently and was detected in almost one-third of the days in a month. From the observation with the sky camera, the enhancement occurred owing to the superimposition of the diffuse irradiance scattered at the edges of cumulus clouds near

the sun on the direct irradiance passing through a gap in the clouds. It is also found that the enhancement is induced when the cumulus or cumulonimbus clouds generated along meteorological fronts pass near the site. Events with enhanced solar irradiance were detected for five months and their amplifications, durations, and volumes were analyzed statistically. The amplifications of some of the largest enhancement events exceeded 1.6, and their durations were several tens of seconds or several minutes. Statistical analyses showed events with either large amplifications or long durations, but not events with both large amplifications and long durations were found.

In Chapter 6, characteristics of *TI* and *Max*.*NU* of solar irradiance and also their relationship were discussed on the basis of field observations in which the timescale is several seconds or less and the area is about the size of the PV module. The use of repeated measurements with a single PVMS is proposed to detect stable irradiance events in time and space for high-accuracy outdoor PV module performance characterizations. The use of repeated measurements with a single PVMS is proposed to detect stable irradiance events in time and space for high-accuracy outdoor PV module performance characterizations. In the repeated measurements of solar irradiance, the characteristics of temporal instability and maximum nonuniformity were examined on the basis of the distance between two PVMSs, measurement time, repeated count, and time interval between measurements. It was found that temporal instability increases with measurement time or repeated count. Also, the maximum nonuniformity increases when the distance between two PVMSs increases. The effect of time interval on temporal instability or nonuniformity is not very obvious. The repeated measurements with a measurement time of 200 ms and a repeat count of 5 are applied to widely strongly fluctuating solar irradiance observed under numerous cumulous clouds and

gaps. The events detected under the condition of *TI* less than 1% satisfy the condition of *Max*.*NU* less than 1%. This means that the events in which irradiance is stable and uniform can be detected only by referring to *TI* obtained by repeated measurements with a single PVMS. This finding indicates that repeated measurements can be employed as a filtering method for monitoring irradiance conditions for high-accuracy outdoor PV module performance characterizations.

Acknowledgements

I would like to express my gratitude to all those who helped and encouraged me to complete this dissertation.

I would like to express my greatest gratitude to my academic advisors, Prof. Tomonao Kobayashi at Graduate School of Engineering, Gifu University for his patience, motivation, enthusiasm, immense knowledge and assistance throughout my doctoral degree study in the lab, my daily life and job hunting, best supervision and supporting me during my study. Without his patient instruction, insightful criticism and expert guidance, I could not finish my thesis.

I would like to thank Assoc. Prof. Jun Yoshino who gives me a lot of valuable suggestions and supports for my study and job hunting. His guidance also contributed to this research.

I express my sincere thanks to Prof. Ichiro Tamagawa for the evaluation of the thesis and for his valuable comments and advices.

I would like to thank the researcher Yoshihiro Hishikawa and Takuya Doi who belong to the National Institute of Advanced Industrial Science and Technology (AIST), Thank you for your comment and help in the successful publication of papers.

I also want to thank all the teachers, especially Prof. Li Fusheng, Assoc. Prof. Wei Yongfen, Assistant Prof. Yasushi Ishiguro, and staffs of BWEL Program of Gifu University who always supported my study. The BWEL program provided an invaluable platform for me to broaden my horizons.

I want to say my special thanks to Yasuyo Yamada for your help with documents-related things. You always listen carefully to my troubles and gave me valuable advices. Thank you for your kindness.

I greatly appreciate the important assistance and help from all members from the Natural Energy Laboratory during my study in Gifu University in this six years. I have not only received help in my professional knowledge, but also in Japanese study as well as in my daily life. I could not be in this stage without receiving help and assistance from all of you. Thank you for giving me such a valuable time in laboratory.

I would like to give my very special and gratitude to my husband, my parents, my brothers, my big families, and my friends, who have been supporting me in each and every step I take. Thank you for your patiently listening, understanding, support and encouragement.

This work is performed under the project “Development of precise PV performance characterization technologies” supported by New Energy and Industrial Technology Development Organization (NEDO) under the Ministry of Economy, Trade and Industry (METI). I express my grateful thanks for your support.

Finally, I am very sorry that I am not able to mention all people who have given a contribution to this thesis. I am sure that some people will be missing to be mentioned. I would like to thank all of you.